

AD-A064 048

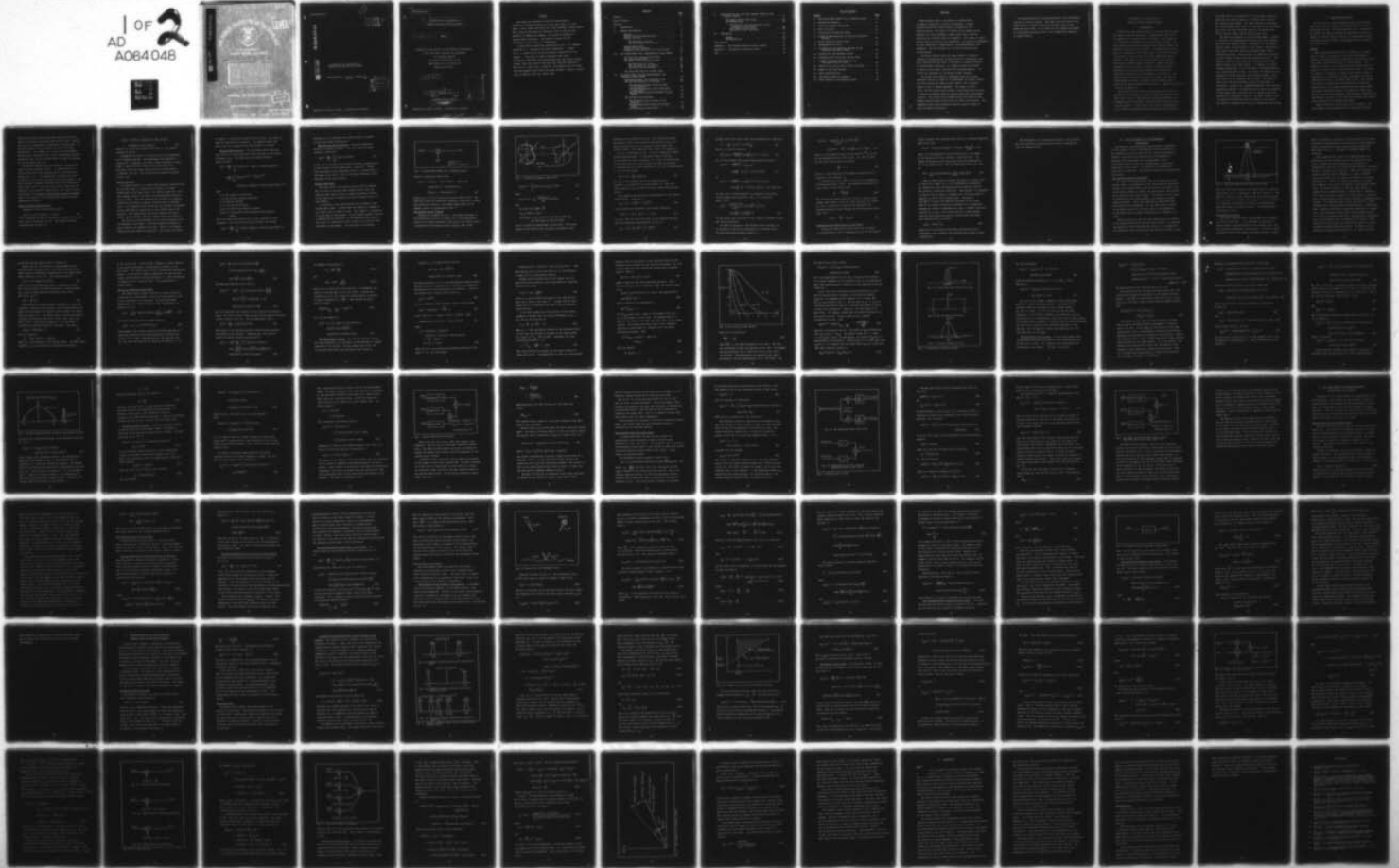
AIR FORCE INST OF TECH WRIGHT-PATTERSON AFB OHIO SCH--ETC F/G 17/8  
AN ANALYSIS OF THE EFFECTS OF SPECKLE ON LASER SCANNING SYSTEMS--ETC(U)  
DEC 78 B W NEWTON

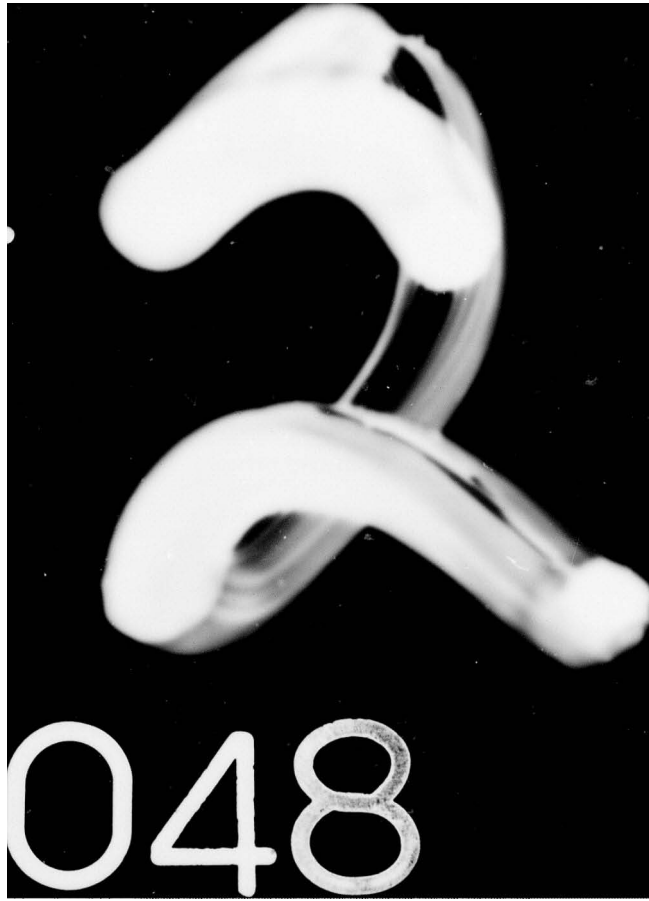
UNCLASSIFIED

AFIT/GE0/EE/78-3

NL

1 OF 2  
AD  
A064 048





AD A064048

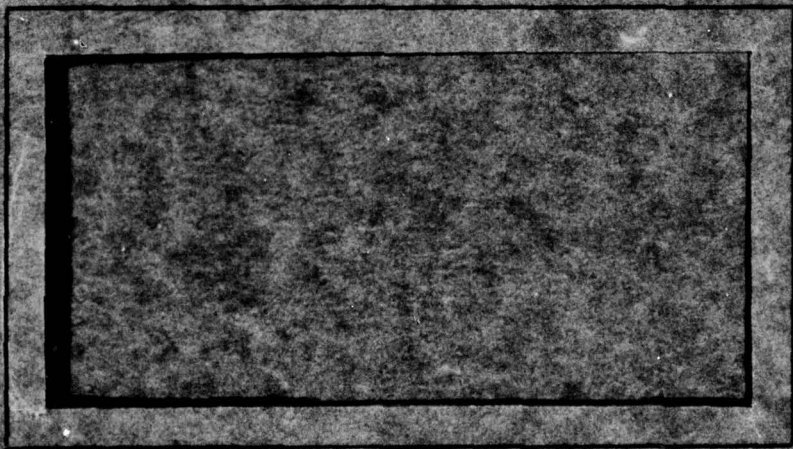
DDC FILE COPY

# AIR FORCE INSTITUTE OF TECHNOLOGY



LEVEL 4

AIR UNIVERSITY  
UNITED STATES AIR FORCE



SCHOOL OF ENGINEERING

WRIGHT-PATTERSON AIR FORCE BASE, OHIO

DDC  
JAN 31 1979  
A

DISTRIBUTION STATEMENT A

Approved for public release;  
Distribution Unlimited

79 01 30 149

AFIT/GEO/EE/78-3

①

LEVEL #

AD A064048

DDC FILE COPY.

AN ANALYSIS OF THE EFFECTS OF  
SPECKLE ON LASER SCANNING SYSTEMS

AFIT/GEO/EE/78-3 BILLY W. NEWTON, Jr.  
2nd Lt. USAF

DDC  
RECEIVED  
JAN 31 1979

A

Approved for public release; distribution unlimited.

79 01 30 149

14

AFIT/GEO/EE/78-3

6 AN ANALYSIS OF THE EFFECTS OF SPECKLE ON LASER SCANNING SYSTEMS.

9 - Master's THESIS

Presented to the Faculty of the School of Engineering of the Air Force Institute of Technology Air Training Command in Partial Fulfillment of the Requirements for the Degree of Master of Science

12 106p.

10 by Billy W./Newton, Jr., B. S. 2nd Lt USAF Graduate Electro-Optics

11 December 1978

ADDITIONAL TO	
DATE	DATE INDEXED <input checked="" type="checkbox"/>
CUE	DATE INDEXED <input type="checkbox"/>
UNCLASSIFIED	<input type="checkbox"/>
IDENTIFICATION	
BY	
AFIT DIVISION/AVAILABILITY CODES	
DATE	AVAIL. and/or SPECIAL
A	

Approved for public release; distribution unlimited

012 225 Gu

## Preface

This paper was sponsored by the Air Force Avionics Laboratory at Wright-Patterson Air Force Base, Ohio. In this paper a laser system consisting of a laser scanning a rough surface and a receiver measuring the reflected field is used for the purposes of imaging and ranging. The system is modeled by second moment techniques. The effect of speckle on the performance of the system is investigated.

I would like to express my appreciation to Dr. P. S. Maybeck and Major R. J. Carpinella for their suggestions. I thank Dr. B. L. Sowers of the Air Force Avionics Laboratory for his support. I also wish to thank Lieutenants Paul Idell, Pat Martone, Bob Mason, and John Santiago for their moral support without which this thesis would have been much more difficult. Most of all I would like to thank Dr. Stan Robinson for his ideas and encouragement which made this paper possible. Finally I would like to thank my typist Ms. Sheri Vogel.

## CONTENTS

	<u>Page</u>
Preface . . . . .	ii
List of Figures . . . . .	v
Abstract . . . . .	vi
I. INTRODUCTION . . . . .	1
II. GENERAL CONFIGURATION . . . . .	3
Speckle . . . . .	3
Complex Baseband Representation . . . . .	4
Optical Receivers . . . . .	5
The Heterodyne Receiver . . . . .	6
The Direct Detection Receiver . . . . .	7
Second Moment Model . . . . .	7
Huygens-Fresnel Integral . . . . .	8
Propagation and Reflection of a Laser Field . . . . .	12
III. THE SYSTEM MODELS FOR A MONOCHROMATIC LASER SOURCE . . . . .	15
The Line Scan Imaging System Model . . . . .	15
The Rough Surface Model . . . . .	16
The Direct Detection Current Model . . . . .	19
The Mean Detector Current . . . . .	21
The Covariance of the Current . . . . .	28
The Direct Detection Model . . . . .	33
The Heterodyne Receiver Current Model . . . . .	38
IV. THE SYSTEM MODELS FOR QUASIMONOCHROMATIC AND BROADBAND LASER SOURCES . . . . .	45
Quasimonochromatic and Broadband Fields . . . . .	45
The Quasimonochromatic System Models . . . . .	47
The Quasimonochromatic Field Incident on the Detector . . . . .	47
The Quasimonochromatic-Direct Detection Current Model . . . . .	48
The Quasimonochromatic-Heterodyne Current Model . . . . .	49
The Broadband System Models . . . . .	50
The Broadband Field Incident on the Detector . . . . .	50
The Broadband-Direct Detection Current Model . . . . .	55
The Heterodyne Current Model . . . . .	57

V.	APPLICATION OF THE LINE SCAN IMAGING SYSTEM TO THE RANGING PROBLEM . . . . .	61
	The Ranging Method and System . . . . .	61
	The Ranging Model . . . . .	62
	The Modulated Quasimonochromatic Field	
	Incident on the Detector . . . . .	63
	The Ranging Current Model . . . . .	68
	Detection of the Time Delay . . . . .	77
VI.	CONCLUSIONS . . . . .	83
	Summary . . . . .	83
	Recommendations . . . . .	85
	Bibliography. . . . .	87
	Appendix A: The Extended Huygens-Fresnel Integral . . . . .	89
	Appendix B: The Method of Stationary Phase . . . . .	93
	Vita . . . . .	95



## List of Figures

<u>Figure</u>	<u>Page</u>
1. The Second Moment Model for an Unknown Current . . .	8
2. Diffraction Geometry . . . . .	9
3. Line-Scan Imaging System Model . . . . .	16
4. Plot of $P_{\rho}(\alpha-\beta)$ . . . . .	25
5. Illustration of Function Widths . . . . .	27
6. Graphical Representation of Current Correlation Distance. . . . .	32
7. Direct Detection Current Model . . . . .	36
8. Determination of $A^2(t)$ . . . . .	40
9. The Model for the Amplitude Squared of the Heterodyne Receiver Current . . . . .	43
10. Notation for the Broadband System . . . . .	51
11. Broadband-Direct Detection Current Model . . . . .	57
12. Temporal Frequency Spectrums for the Heterodyne Receiver Fields . . . . .	64
13. Values of $f_{IF}$ and $f_c$ which Prevent Aliasing . . . . .	67
14. Model of the Total Current . . . . .	72
15. Noise Representation . . . . .	75
16. The Current Model for Ranging . . . . .	77
17. Phase Diagram of the Ranging Current . . . . .	80

## Abstract

When coherent light is incident on a surface which is rough in comparison to optical wavelengths, a random interference pattern called speckle is produced in the reflected field. The effects of speckle on an imaging system composed of a laser scanning a rough surface and a receiver measuring the reflected field are examined. Three types of lasers and two types of receivers are considered. The lasers are designated by their bandwidths as monochromatic, quasimonochromatic, and broadband. The two receivers are the direct detection and the heterodyne.

The field reflected from the rough surface is "crudely" modeled by multiplying the incident field by a reflectance term and a random phase term which is indicative of speckle effects. By second moment techniques, the imaging systems are modeled in terms of their mean, covariance and system parameters. All fields are propagated by the Huygens-Fresnel integral.

The system consisting of a broadband laser and a direct detection receiver is shown to be independent of speckle effects. All other systems are shown to have "noise", due to speckle effects, which is signal dependent. The signal to noise ratio, for the systems which include a direct detection receiver, is found to be greater than for systems which have a heterodyne receiver. The systems with broadband lasers are shown to have higher resolution than systems with the other laser sources. The broadband laser-direct detection receiver system is found to have the highest resolution.

A system consisting of a quasimonochromatic laser-heterodyne receiver is used for ranging. The range from the system to the rough surface is found by measuring the phase delay in the reflected laser field. It is found that the ranging performance of a heterodyne scanning system is not fundamentally degraded by speckle effects.

AN ANALYSIS OF THE EFFECTS OF  
SPECKLE ON LASER SCANNING SYSTEMS

I. Introduction

A laser line-scan imaging system is a system which produces the image of some desired object. Fundamentally, the system is composed of a transmitter and a receiver. The transmitter is a laser which illuminates the desired object surface. The laser field is reflected or backscattered from the surface and partially collected by the receiver. The backscattered field, which is a function of the reflectivity of the object surface, is processed by the receiver to form an image of the object surface. This image is the desired output of the receiver. The receiver contains optics, detectors, filters, and other components which are needed to produce the desired image. A drawback to this system occurs because most surfaces are rough when compared to the wavelength of a laser field. The rough surface introduces noise into the image. For coherent illumination this noise is commonly called speckle, and it distorts the image obtained by the receiver. Speckle is discussed in detail in Chapter II.

The purpose of this thesis is to determine the effects of speckle on the performance of a laser line-scan imaging system. Three laser sources: monochromatic, quasimonochromatic, and broadband; and two receivers: heterodyne and direct detection are investigated. In this thesis, the effect of propagation on all fields is determined from the Huygens-Fresnel integral.

The rough surface is represented by a well known statistical model and the receiver output is a current which is based on a known receiver model. The output current is described by a second moment model which is a function of the laser beam spot size, the system scanning velocity, the surface area of the receiver input, and the type of laser used.

The thesis is organized in the following manner. Chapter II develops the background material necessary for examining the line-scan imaging systems. In Chapter III, the second moments models are determined for two systems: monochromatic laser-direct detection receiver and monochromatic laser-heterodyne receiver. These systems are compared on the basis of their signal to noise ratio and resolution ability. This chapter establishes the method for determining the second moment models of the other systems. In Chapter IV, linear frequency modulation is used to produce a quasimonochromatic and a broadband laser source. The results of Chapter III are extended to produce four more second moments models, which arise from the two modulated laser sources. The signal to noise ratio and the resolution ability of each model is discussed. In Chapter V, a quasimonochromatic laser source is amplitude modulated. The modulated laser field is propagated to the rough surface and back, and its change in phase is measured by a heterodyne receiver. The phase change is used to determine the distance from the surface to the system. The effects of quantum noise are also included in this system.

## II. General Configuration

In this chapter, several background areas are discussed. These areas serve as a basis for examining the laser line-scan imaging system. The background areas are: a discussion of speckle, the complex baseband representation for optical fields, the optical receiver models, the second moment model, the Huygens-Fresnel integral, and propagation and reflection of a laser field.

### Speckle

When a coherent optical field is incident on a surface which is rough in comparison to the optical wavelength, a random interference pattern is produced in the reflected field. This random interference pattern is called speckle. One example of speckle is the sparkling pattern produced when the light of a visible laser is reflected from a wall. The effect of speckle is to degrade the image of the object surface by superimposing a "noiselike structure which masks the spatial information present in the image" (Ref 1:1257). This results in a pattern of constructive and destructive interference being produced in the light reflected from the rough surface. The random interference pattern is composed of bright spots due to constructive interference, dark spots due to destructive interference, and areas with intensities between these extremes. Thus the pattern has a granular appearance.

Rough surfaces are not the only cause of speckle. The term speckle has been generalized to include most spatial

interference effects that result when any type of wave or field is scattered from diffuse objects (Ref 2:16). Speckle also occurs in atmospheric transmissions and holography. It was once thought to be a nuisance, but now it has many applications. For example, it is used in the measurement of motion of a rough body (Ref 1:1271), photographic optical processing (Ref 1:1275), and the remote sensing of crosswind in the atmosphere (Ref 3:1).

The speckle phenomena has been known and investigated since the time of Newton (Ref 4). Its early history is briefly discussed in the introduction of a book edited by Dainty (Ref 5:1-7). The invention of the first CW laser in 1960 led to the first observations of laser speckle. They were reported by Rigden and Gordon (Ref 6:2367-2368) and by Oliver (Ref 7:220). Since the early 1960's, much work has been done in the speckle related field. The entire issue of the November 1976 Journal of the Optical Society of America (Ref 1) was devoted to the discussion of numerous speckle phenomena and effects.

#### Complex Baseband Representation

Consider the real scalar optical field

$$u(\bar{r}, t) = A(\bar{r}, t) \cos[2\pi f_0 t - \phi(\bar{r}, t)] \quad (1)$$

It is a function of time,  $t$ , and space,  $r$ , where  $\bar{r}$  is a vector with spatial coordinates  $(x, y, z)$ . The complex baseband representation of  $u(\bar{r}, t)$  is

$$u(\bar{r},t) = \text{Re}\{A(\bar{r},t) \exp[j\phi(\bar{r},t)] \exp[-j2\pi f_0 t]\}$$

$$\triangleq \text{Re}\{U(\bar{r},t) \exp[-j2\pi f_0 t]\} \quad (2)$$

where  $\text{Re}\{\cdot\}$  is the real operator and  $U(\bar{r},t)$  is the complex envelope of  $u(\bar{r},t)$ .

Throughout this thesis, the field,  $u(r,t)$ , is represented by its complex envelope. The exponential time function is suppressed. In addition, the field is often described at some plane  $z$ , thus it varies in the  $x$  and  $y$  directions only. Therefore, the real scalar optical field at a given plane  $z$  is denoted  $U(x,y,t)$ . The real field can always be obtained from Eq. (2).

### Optical Receivers

An optical receiver is a device which measures optical fields. The receiver input is a field and its output is a signal proportional to the input field. The receiver input for a line-scan imaging system is the laser field backscattered from the object surface. The field entering the receiver is in general limited by the receiver's optics, field-of-view, or detector area. It is assumed in this thesis that the receiver is designed so that the field is limited only by the surface area of the detector. This insures that the entire image of the object surface and its spatial frequency content enters the receiver.

Two receivers, the heterodyne and the direct detection, are investigated in this paper. With the exception of Chapter V, both receivers are assumed to be ideal. That is, all quantum effects and noise terms are neglected. This allows the effects



of speckle on the receiver output to be isolated. This does not make the problem any less general. The quantum effects and noise terms can be added to the final results if desired.

The Heterodyne Receiver. The heterodyne system adds the input field to a local oscillator field centered at the optical frequency  $f_o - f_{IF}$ . The ideal receiver output current is (Ref 8:481-487)

$$\begin{aligned}
 i(t) &= \frac{q\eta}{hf_o} \int \int_{A_d} |U_s(x,y,t) + U_{LO}(x,y) \exp[j2\pi f_{IF}t]|^2 dx dy \\
 &= \frac{q\eta}{hf_o} \int \int_{A_d} [ |U_s(x,y,t)|^2 + |U_{LO}(x,y)|^2 \\
 &\quad + 2\text{Re}\{U_s(x,y,t)U_{LO}^*(x,y) \exp[-j2\pi f_{IF}t]\} ] dx dy \quad (3)
 \end{aligned}$$

where

$q$  is the charge of an electron

$\eta$  is the detector quantum efficiency

$h$  is Planck's constant

$f_o$  is the optical frequency

$A_d$  is the area of the detector surface

$U_s(x,y)$  is the signal field incident on the detector surface

The first and second terms in Eq. (3) are centered at zero frequency. They can be electrically filtered out leaving

$$i_h(t) = \frac{2q\eta}{hf_o} \int \int_{A_d} \text{Re}\{U_s(x,y)U_{LO}^*(x,y) \exp[-j2\pi f_{IF}t]\} dx dy \quad (4)$$

From Eq. (4) it is seen that the output current is related to the actual input field  $U_s(x,y)$ .

The Direct Detection Receiver. The direct detection system is a square law device. The ideal receiver output current is (Ref 9:91)

$$i_d(t) = \frac{qn}{hf_0} \int \int_{A_d} |U_s(x,y,t)|^2 dx dy \quad (5)$$

In Eq. (5) it is seen that the output current is proportional to the intensity of the input field,  $|U_s(x,y)|^2$ . Recall that the output of the heterodyne receiver is proportional to the input field itself. This is the major difference in the mechanics of the two receivers.

#### Second Moment Model

The input field to the optical receiver may be unknown. This is true for the case where speckle occurs since the receiver input field contains a random interference pattern. If the input field is unknown the receiver output current is also unknown.

In statistics, one representation for an unknown is the second moment model. In this model the unknown is thought of as a signal plus an additive noise. The "signal" is considered to be the mean of the unknown. For an unknown current, the mean is denoted  $E[i(t)]$  where  $E[\cdot]$  is the expected value operator. The "noise" is considered to have a mean of zero and the same covariance as the unknown. The covariance of an unknown

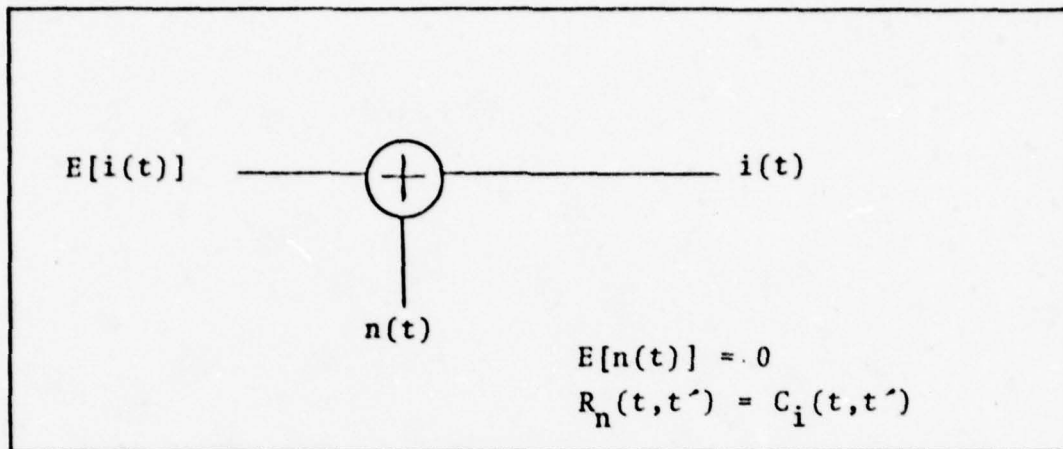


Fig. 1 Second Moment Model for an Unknown Current

current is defined as (Ref 10:321)

$$\begin{aligned}
 C_i(t, t') &= E[(i(t) - E[i(t)])(i(t') - E[i(t')])] \\
 &= E[i(t)i(t')] - E[i(t)]E[i(t')] \\
 &\triangleq R_i(t, t') - E[i(t)]E[i(t')] \qquad (6)
 \end{aligned}$$

where  $R_i(t, t')$  is the correlation function (Ref 11:337). The period for which the correlation function is non-zero is called the correlation interval. The second moment model for an unknown current is illustrated in Fig. 1.

#### The Huygens-Fresnel Integral

Consider the geometry of Fig. 2. The complex envelope of the monochromatic field at a point  $(x, y)$  in the observation plane due to complex envelope of the field in the object plane is expressed by the Huygens-Fresnel integral (Ref 12:58)

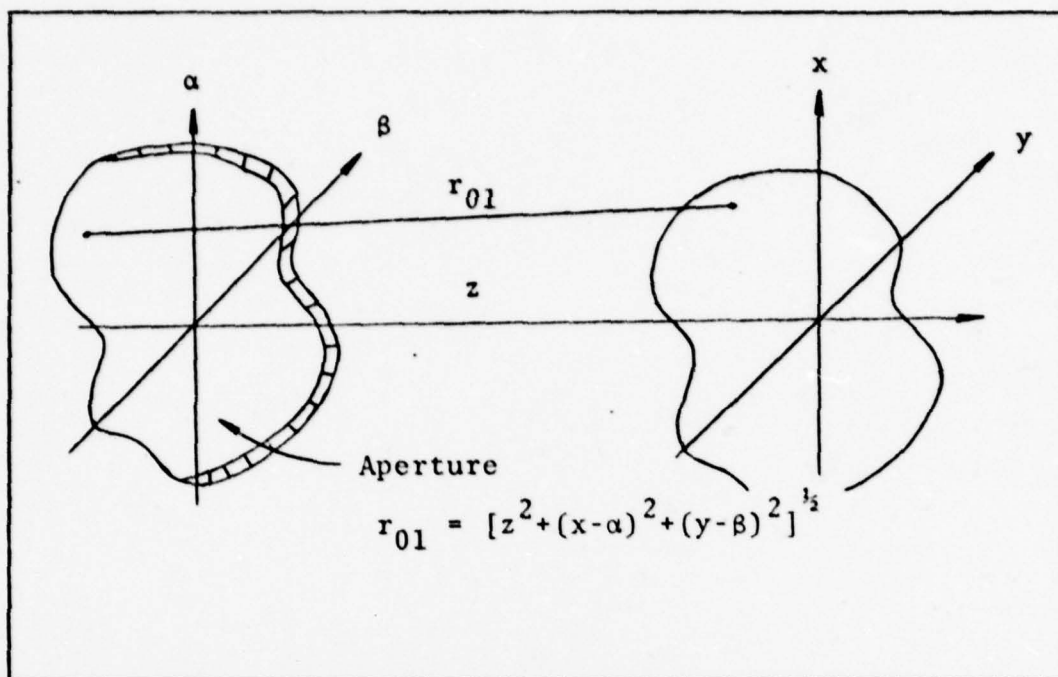


Fig. 2 Diffraction Geometry (Ref 12:57)

$$U_2(x,y) = \int_{-\infty}^{\infty} \int_{-\infty}^{\infty} h(x,y,\alpha,\beta) U_1(\alpha,\beta) d\alpha d\beta \quad (7)$$

where

$$h(x,y,\alpha,\beta) = \frac{1}{j\lambda} \frac{\exp[jkr_{01}]}{r_{01}} \cos(\bar{n}, \bar{r}_{01}) \quad (8)$$

and

$k$  is the wave number,  $\frac{2\pi}{\lambda}$

$r_{01}$  is shown in Fig. 2

$\cos(\bar{n}, \bar{r}_{01})$  is the cosine of the angle between  $\bar{r}_{01}$  and the normal to the  $\alpha$ - $\beta$  plane.

Eq. (7) is valid for monochromatic fields only. The finite extent of the field in the  $\alpha, \beta$  plane is included in the

mathematical description of  $U(\alpha, \beta)$ . This restriction allows the infinite limits to be placed on the integral in Eq. (7). Unless otherwise noted, all integrals in this paper have infinite limits. For simplicity these limits are suppressed.

Eq. (7) is difficult to use. It can be simplified through several approximations. If the angle between  $\bar{n}$  and  $\bar{r}_{01}$  is less than  $18^\circ$ , then  $\cos(\bar{n}, \bar{r}_{01}) \approx 1$ . Also, if the deviation of the field from the  $z$  axis is much less than the distance  $z$ , the quantity  $r_{01}$  in the denominator of Eq. (8) is approximately  $z$ . Eq. (8) now becomes

$$h(x, y, \alpha, \beta) \approx \frac{1}{j\lambda z} \exp[jkr_{01}] \quad (9)$$

The  $r_{01}$  in the exponent can not be approximated by  $z$  because it is multiplied by a large number,  $k$ . Thus even small changes in  $r_{01}$  can result in phase changes much greater than  $2\pi$ .

One commonly used exponential approximation is the Fresnel approximation. From Fig. 2

$$r_{01} = z \left[ 1 + \left( \frac{x-\alpha}{z} \right)^2 + \left( \frac{y-\beta}{z} \right)^2 \right]^{1/2} \quad (10)$$

In the Fresnel approximation, the binomial expansion,

$$[1+b]^{1/2} = 1 + \frac{1}{2} b - \frac{1}{8} b^2 + \dots \quad |b| < 1 \quad (11)$$

is used. Only the first two terms in the expansion are kept. Thus the exponential approximation for  $r_{01}$  is

$$r_{01} = z \left[ 1 + \frac{1}{2} \left( \frac{x-\alpha}{z} \right)^2 + \frac{1}{2} \left( \frac{y-\beta}{z} \right)^2 \right] \quad (12)$$

Goodman (Ref 12:59) states that this approximation is good when

$$z^3 \gg \frac{\pi}{4\lambda} [(x-\alpha)^2 + (y-\beta)^2]_{\max}^2 \quad (13)$$

Now Eq. (9) can be written as

$$h(x,y,\alpha,\beta) \approx \frac{\exp[jkz]}{j\lambda z} \exp\left[\frac{jk}{2z}[(x-\alpha)^2 + (y-\beta)^2]\right] \quad (14)$$

Eq. (7) then becomes the Fresnel approximation written as

$$U_2(x,y) = \frac{\exp[jkz]}{j\lambda z} \iint U_1(\alpha,\beta) \exp\left[\frac{jk}{2z} [(x-\alpha)^2 + (y-\beta)^2]\right] d\alpha d\beta \quad (15)$$

or

$$U_2(x,y) = \frac{\exp[jkz]}{j\lambda z} \exp\left[j\frac{k}{2z}(x^2+y^2)\right] \iint U_1(\alpha,\beta) \exp\left[j\frac{k}{2z}(\alpha^2 + \beta^2)\right] \exp\left[-j\frac{k}{z}(x\alpha + y\beta)\right] d\alpha d\beta \quad (16)$$

In many cases, field propagation is adequately described by the one dimensional form of Eq. (16). It is given by (Ref 13:316)

$$U_2(x) = \frac{\exp[j(kz - \pi/4)]}{(\lambda z)^{1/2}} \exp\left[j\frac{kx^2}{2z}\right] \int U_1(\alpha) \exp\left[j\frac{k\alpha^2}{2z}\right] \exp\left[-j\frac{2\pi x\alpha}{\lambda z}\right] dx \quad (17)$$

In the latter case, the field at the z plane is variable in only one lateral direction.

As shown in Appendix A, the Huygens-Fresnel integral can be extended to include the propagation of broadband fields. The one dimensional extended integral is

$$U_2(x,t) = \frac{\exp[j(kz - \frac{\pi}{4})]}{(\lambda z)^{\frac{1}{2}}} \exp[jk \frac{x^2}{2z}] \int \int U_1(\alpha, t - \frac{r_{01}}{c}) \exp[j\frac{kx^2}{2z}] \exp[-j2\pi\frac{\alpha x}{\lambda z}] d\alpha \quad (18)$$

where  $c$  is the speed of light and the quantity  $r_{01}/c$  is due to the propagation delay of the field. Eq. (18) is valid for all time varying fields as long as

$$\frac{B}{f_0} \gg 1 \quad (19)$$

where  $B$  is the bandwidth of the complex envelope which is centered at the frequency  $f_0$ .

A special case of Eq. (18) is valid for the propagation of quasimonochromatic fields. The bandwidth restriction on these fields is that (Ref 12:108)

$$\frac{1}{B} \gg \frac{|\bar{r}_{01}|_{\max}}{c} \quad (20)$$

This restriction implies that for a fixed  $\alpha$ ,  $U(\alpha, t)$  cannot change significantly in any time much less than  $1/B$  seconds. Eq. (18) is modified to represent the propagation of quasimonochromatic fields through the following substitution (Ref 12:55)

$$U_1(\alpha, t - \frac{r_{01}}{c}) = U_1(\alpha, t) \quad (21)$$

#### Propagation and Reflection of a Laser Field

Siegman has shown (Ref 14:306) that when the output of a monochromatic laser is propagated by use of the Huygens-

Fresnel Integral, the resulting laser field is a Gaussian spherical wave of the form

$$U(\alpha, \beta) = A \exp[jkz] \exp\left[j \frac{k}{2z} (\alpha^2 + \beta^2)\right] \exp\left[-\frac{\alpha^2 + \beta^2}{W^2(z)}\right] \quad (22)$$

where  $A$  is the amplitude of the field and  $W(z)$  is the radius of the beam spot size at a distance  $z$  from the laser. The radius is measured at the point where the field amplitude is  $e^{-1}$  of its maximum value. The one dimensional form of Eq. (22) is

$$U(\alpha) = \frac{A}{(\lambda z)^{1/2}} \exp\left[j\left(kz - \frac{\pi}{4}\right)\right] \exp\left[-\frac{\alpha^2}{W^2(z)}\right] \exp\left[j \frac{k}{2z} \alpha^2\right] \quad (23)$$

When the above field is normally incident on a surface that is smooth with respect to  $\lambda$ , it is reflected by conjugating the exponential terms and multiplying the resulting field by the surface's reflection coefficient. When  $\exp[jkz]$  is conjugated, it implies that the field is propagating in a direction which is opposite to that of the incident field. Conjugating  $\exp\left[j \frac{k}{2z} x^2\right]$  inverts the spherical wavefront of the field. Some of the incident field may be absorbed by or transmitted through the surface. To represent this loss, a surface reflection coefficient is used. This coefficient has a value between zero (no field reflected) and one (entire field reflected). The reflected field is written

$$U_r(\alpha) = a(\alpha) U_i^*(\alpha) \quad (24)$$

where  $a(\alpha)$  is the surface reflection coefficient and the subscripts  $r$  and  $i$  indicate the reflected and incident fields, respectively.



The development of the background material is now complete. The ideas and theory discussed here are used to examine the line scan imaging system.

### III. The System Models for a Monochromatic Laser Source

The method for determining the system models is developed in this chapter. First a representation for the mechanics of the imaging system is discussed and the rough surface model is defined. These ideas are combined with the background to determine the system models for a monochromatic laser-heterodyne receiver system and a monochromatic laser-direct detection receiver system. For simplicity, the models are found for one dimension. Two dimension models are straightforward but tedious.

#### The Line Scan Imaging System Model

In a line scan imaging system, the laser scans across some object surface. The mechanics of the system keep the detector's surface area aligned normal to the direction of the laser field. As the object surface is scanned, the angle between the incident laser field and the surface changes. The analysis of the system is simplified if the system mechanics and change in incident angle are ignored. These two conditions are satisfied under the following two assumptions: (1) the laser field is normal to the object surface at all times, and (2) the propagation of the laser field is normal to the detector's surface at all times.

During typical use, the line scan imaging system is mounted in an airplane which flies over the object surface. To represent the movement of the system past the surface it is assumed that the coordinate system of the laser and receiver is fixed in space,

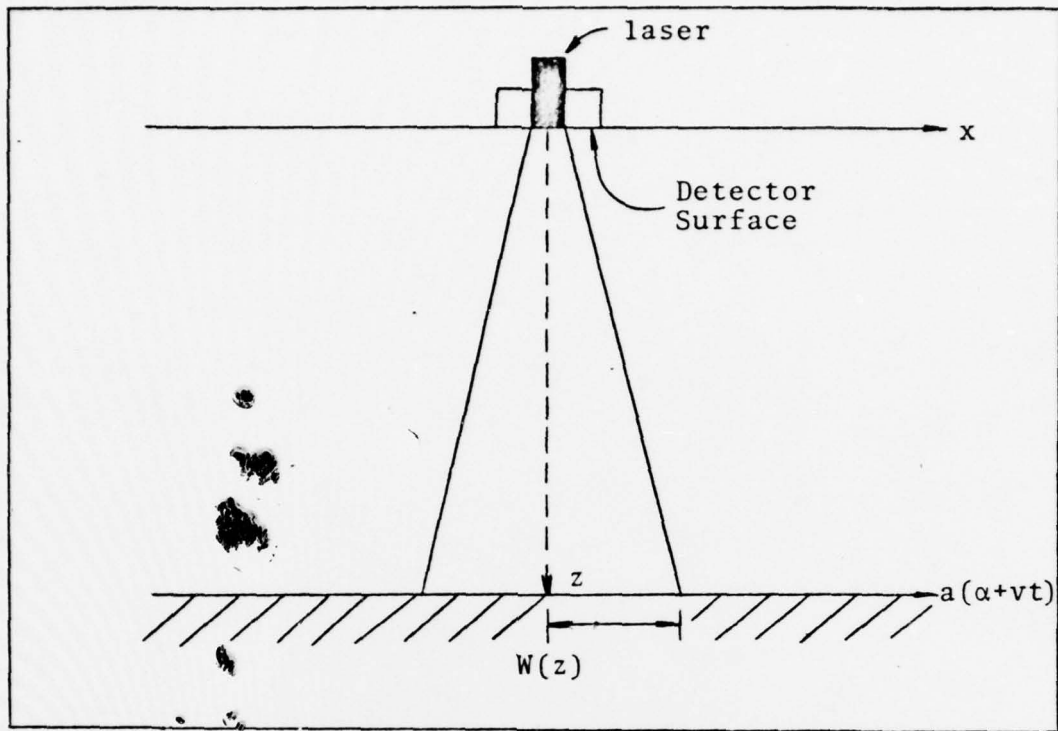


Fig. 3 Line Scan Imaging System Model (Ref 16:28)

while the coordinate system of the surface and its reflection coefficient,  $a(x)$ , is traveling in time with velocity  $v$ . The model is a function of the velocity and the laser beam width,  $W(z)$ , at the object surface. By varying these two parameters, it is possible to determine the effects of spreading beam width and changes in surface velocity. The system model is illustrated in Fig. 3.

#### The Rough Surface Model

The field reflected from a rough surface is, in general, difficult to determine. It is dependent on variations in surface height, the polarization of the incident field, and the reflection coefficient of the surface. In order to avoid a detailed study of the surface scattering problem, a simple

model is developed to represent the rough surface (For a deeper mathematical understanding of the properties of electromagnetic fields scattered from a rough surface consult Beckman and Spizzichino (Ref 17)). The model is developed under five conditions.

First, depolarization effects are ignored because the polarization of the incident field is not included in this thesis. Second, multiple scattering at the surface is insignificant since only the field reflected normal to the object surface is incident on the detector. These two conditions are typically ignored (Ref 17: Chapters 1, 3, and 5; 18:1689) since their effects are very small and difficult to describe mathematically. Third, the surface is assumed to be rough when compared to the optical wavelength so that speckle effects occur. The fourth condition is that the rough surface is thought of as a random variation in height (Ref 17: Chapter 3). This allows the surface roughness to be described by statistics. Also, a field incident on this surface undergoes a random variation in phase. The reflected field is then equivalent to a field reflected from a smooth surface and multiplied by a random phase term. Finally, the surface's reflection coefficient is assumed to be a real function of space with a value between zero and one so that it attenuates the field. The reflection coefficient,  $a(\alpha)$ , is the quantity that is measured by the system. These conditions are the same as the ones used by Lyons in a similar heterodyne imaging problem (Ref 16:21). The model is also similar to the ones used by Miller, et. al. (Ref 19:779-785)

and Beckman and Spizzichino (Ref 17: Chapter 5).

Recall that Eq. (24) describes a monochromatic field reflected from a smooth surface. The field reflected from a rough surface is determined by applying the five rough surface model conditions to Eq. (24). The reflected field is

$$U_r(\alpha) = a(\alpha) \exp[j\theta(\alpha)] U_i^*(\alpha) \quad (25)$$

where  $\theta(\alpha)$  is the random phase and is a function of space. The relation between the random variations in surface height,  $H(x)$ , and the random phase was previously shown to be (Ref 20:36; 21:157)

$$\theta(\alpha) = \frac{4\pi}{\lambda} H(\alpha) \quad (26)$$

The variation in surface height is modeled as a zero mean, stationary, Gaussian random process. The zero mean implies the point that the heights are measured from is chosen in a manner such that  $E[H(\alpha)] = 0$ . The rough surface is often described by a Gaussian distribution (Ref 5:65; 1:1153, 1195, 1205, 1212, 1224; 17:80). Using these assumptions, it is possible to determine the mean and variance of the phase. The mean is

$$E[\theta(\alpha)] = \frac{4\pi}{\lambda} E[H(\alpha)] = 0 \quad (27)$$

and the variance is

$$\sigma_\theta^2 = \left(\frac{4\pi}{\lambda}\right)^2 E[H^2(\alpha)] = \left(\frac{4\pi}{\lambda}\right)^2 \sigma_H^2 \quad (28)$$

where  $\sigma_H^2$  is the variance of the surface height. The RMS surface roughness,  $\sigma_H$ , can be compared to the optical wavelength,  $\lambda$ ,

by use of Eq. (28). If the surface roughness is small compared to the optical wavelength, the RMS phase variation,  $\sigma_\theta$ , is also small. This means there is little problem with interference. However, as the surface roughness approaches the optical wavelength, the RMS phase variation approaches  $2\pi$ . Thus interference is produced in the reflected field. This interference is called speckle.

#### The Direct Detection Current Model

The ideal detector output current for a direct detection system can now be determined. Recall that this current is due to the field input to the detector. The one dimensional monochromatic laser field incident on the rough surface is given by Eq. (23)

$$U_i(\alpha) = \frac{A}{(\lambda z)^{1/2}} \exp[j(kz - \frac{\pi}{4})] \exp[-\frac{\alpha^2}{W^2(z)}] \exp[j\frac{k\alpha^2}{2z}] \quad (29)$$

The field reflected from the rough surface is

$$U_r(\alpha) = a(\alpha + vt) e^{j\theta(\alpha+vt)} U_i^*(\alpha) \quad (30)$$

The argument " $\alpha+vt$ " results because the surface and thus its reflection coefficient and height variation is moving with respect to the laser. Substituting Eqs. (29) and (30) into Eq. (17) gives the field at the input to the detector. It is

$$\begin{aligned}
U_d(x) = & \frac{A}{\lambda z} \exp[-j2(kz - \pi/4)] \exp[-jk \frac{x^2}{2z}] \\
& \int a(\alpha+vt) \exp[j\theta(\alpha+vt)] \exp[-\frac{\alpha^2}{W^2(x)}] \\
& \exp[-j\frac{k\alpha^2}{z}] \exp[j2\pi\frac{x\alpha}{\lambda z}] d\alpha
\end{aligned} \tag{31}$$

The magnitude squared of this field is

$$\begin{aligned}
|U_d(x)|^2 = & (\frac{A}{\lambda z})^2 \int \int a(\alpha+vt) a(\beta+vt) \exp[-\frac{\alpha^2 + \beta^2}{W^2(z)}] \\
& \exp[-jk \frac{\alpha^2 - \beta^2}{z}] \exp[j2\pi\frac{x}{\lambda z} (\alpha - \beta)] \\
& \exp[j\theta(\alpha+vt) - j\theta(\beta+vt)] d\alpha d\beta
\end{aligned} \tag{32}$$

Eq. (32) represents the intensity of the field at the detector input. The ideal receiver output current for the direct detection system is given in Eq. (5). Its one dimensional form is

$$i_d(t) = \frac{q\eta}{hf_0} \int P_D(x) |U_s(x)|^2 dx \tag{33}$$

where  $P_D(x)$  is the limiting aperture function which describes the surface of the detector. Combining Eqs. (32) and (33) yields the detector output current which is

$$\begin{aligned}
i_d(t) = & (\frac{A}{\lambda z})^2 \frac{q\eta}{hf_0} \int \int \int P_D(x) a(\alpha+vt) a(\beta+vt) \\
& \exp[-\frac{\alpha^2 + \beta^2}{W^2(x)}] \exp[-jk\frac{\alpha^2 - \beta^2}{z}] \exp[j\frac{2\pi x}{\lambda z} (\alpha - \beta)] \\
& \exp[j(\theta(\alpha+vt) - \theta(\beta+vt))] dx d\alpha d\beta
\end{aligned} \tag{34}$$

To simplify the notation let

$$A_1 = \left(\frac{A}{\lambda z}\right)^2 \frac{qn}{hf_0} \quad (35-a)$$

and

$$h(\alpha) = \exp\left[-\frac{\alpha^2}{W^2(z)}\right] \quad (35-b)$$

where  $h(\alpha)$  is called the system function. It determines the effect of the beam spot size on the system. Solving the  $x$  integration in Eq. (31) yields the spatial Fourier transform of  $P_D(x)$  evaluated at  $f_x = \frac{\alpha-\beta}{\lambda z}$ . The transform of  $P_D(x)$  will be denoted

$$F_x[P_D(x)] \Big|_{f_x = \frac{\alpha-\beta}{\lambda z}} = P_{DF}(\alpha-\beta) \quad (36)$$

Eq. (34) now reduces to

$$i_d(t) = A_1 \iint P_{DF}(\alpha-\beta) a(\alpha+vt)a(\beta+vt) \\ h(\alpha)h(\beta) \exp\left[-jk\frac{\alpha^2-\beta^2}{z}\right] \\ \exp[j(\theta(\alpha+vt)-\theta(\beta+vt))] d\alpha d\beta \quad (37)$$

The Mean Detector Current. Now that the detector current has been determined, it is possible to find the mean or "signal" component of the current. The only random term in Eq. (37) is the phase deviation, thus the mean of the current is



$$E[i_d(t)] = A_1 \int \int P_{DF}(\alpha-\beta) a(\alpha+vt) a(\beta+vt) \\ h(\alpha) h(\beta) \exp[-jk \frac{\alpha^2 - \beta^2}{z}] \\ E[\exp(j(\theta(\alpha+vt) - \theta(\beta+vt)))] d\alpha d\beta \quad (38)$$

The phase deviation,  $\theta$ , is a zero mean Gaussian random process. Therefore the term,  $E[\exp[j(\theta(\alpha+vt) - \theta(\beta+vt))]]$  can readily be determined by use of the characteristic function. A form of the characteristic function (Ref 10:419) is

$$\phi_x(V) = E[e^{jVx}] \quad (39)$$

If  $x$  is a Gaussian random variable, then Eq. (39) becomes

$$\phi_x(V) = \exp[jVE[x] - \frac{v^2 \sigma_x^2}{2}] \quad (40)$$

In Eq. (39) let  $V = 1$  and  $x = \theta(\alpha+vt) - \theta(\beta+vt)$ . Then

$$E[\exp[j(\theta(\alpha+vt) - \theta(\beta+vt))]] = \exp[-\frac{1}{2}(1)^2 \sigma_1^2] \quad (41)$$

where

$$\begin{aligned} \sigma_1^2 &= E[(\theta(\alpha+vt) - \theta(\beta+vt))^2] \\ &= E[\theta^2(\alpha+vt) + \theta^2(\beta+vt) - 2\theta(\alpha+vt)\theta(\beta+vt)] \\ &= 2\sigma_\theta^2 - 2R_\theta(\alpha-\beta) \\ &\triangleq 2\sigma_\theta^2 (1-\rho(\alpha-\beta)) \end{aligned} \quad (42)$$

where  $\rho(\alpha-\beta)$  is the normalized correlation function of the phase  $\theta$ . Eq. (41) now becomes

$$E[\exp[j(\theta(\alpha+vt) - \theta(\beta+vt))]] = \exp[-\sigma_{\theta}^2(1-\rho(\alpha-\beta))] \quad (43)$$

This function has a value of one when  $\alpha-\beta=0$ , and decreases to  $\exp[-\sigma_{\theta}^2]$  as  $\alpha-\beta$  approaches infinity.

Beckman and Spizzichino (Ref 17:81) suggest that the phase correlation function can be represented by a Gaussian function of the form

$$\rho(\alpha-\beta) = \exp\left[-\left(\frac{\alpha-\beta}{r_c}\right)^2\right] \quad (44)$$

where  $r_c$  is the correlation distance of the rough surface when  $\rho(\alpha-\beta)$  drops to the value  $e^{-1}$ . Goodman (Ref 18:1698) states that  $r_c$  is generally less than 0.1mm for optically rough surfaces.

It has been assumed that the deviation of the surface roughness is greater than the optical wavelength or  $\sigma_h > \lambda$ . Eq. (28) can be rewritten as

$$\sigma_{\theta} = \frac{4\pi}{\lambda} \sigma_H > \frac{4\pi}{\lambda} \lambda = 4\pi \quad (45)$$

When  $\sigma_{\theta} > 5$ , the correlation distance of the reflected field is less than the correlation distance of the rough surface by a factor of  $1/\sigma_{\theta}$  (Ref 22:984). Therefore, the field correlation distance,  $l$ , is

$$l < r_c / \sigma_{\theta} = \frac{.1\text{mm}}{4\pi} \approx .01\text{mm} \quad (46)$$

This field correlation distance was previously derived by Lyons (Ref 16:33). Its significance is that it is the maximum

distance that any two points in the reflected field (at the surface) can be separated by and still be correlated. Eq. (43) is now called the field correlation function and is denoted  $P_\ell(\alpha-\beta)$ . That is

$$P_\ell(\alpha-\beta) = \exp[-\sigma_\theta^2(1-\rho(\alpha-\beta))] \quad (47)$$

where  $\ell$  indicates the field correlation distance. Fig. 4 is a plot of  $P_\ell(\alpha-\beta)$  as a function of  $\frac{\alpha-\beta}{r_c}$  for several values of  $\sigma_H$ .

Another simplification to Eq. (38) is the approximation

$$\exp[-j\frac{k}{z}(\alpha^2-\beta^2)] \approx 1 \quad (48)$$

which is valid for the condition of

$$\frac{k}{z}|\alpha^2-\beta^2|_{\max} \ll 1 \quad (49)$$

$|\alpha^2-\beta^2|_{\max}$  occurs when  $\alpha$  takes on its maximum value and  $\beta$  is at its minimum, or vice versa. The maximum value of  $\alpha$  and  $\beta$  is the radius of the beam spot size,  $W(z)$ , on the rough surface. The maximum value that  $\alpha$  and  $\beta$  can be separated and still be correlated (i.e. nonzero) is  $\ell$ , the field correlation distance. Thus

$$\begin{aligned} |\alpha^2-\beta^2|_{\max} &= |(W(z))^2 - (W(z)-\ell)^2| \\ &\approx 2W(z)\ell \end{aligned} \quad (50)$$

Eq. (49) becomes

$$\frac{k}{z} 2W(z)\ell \ll 1 \quad (51)$$

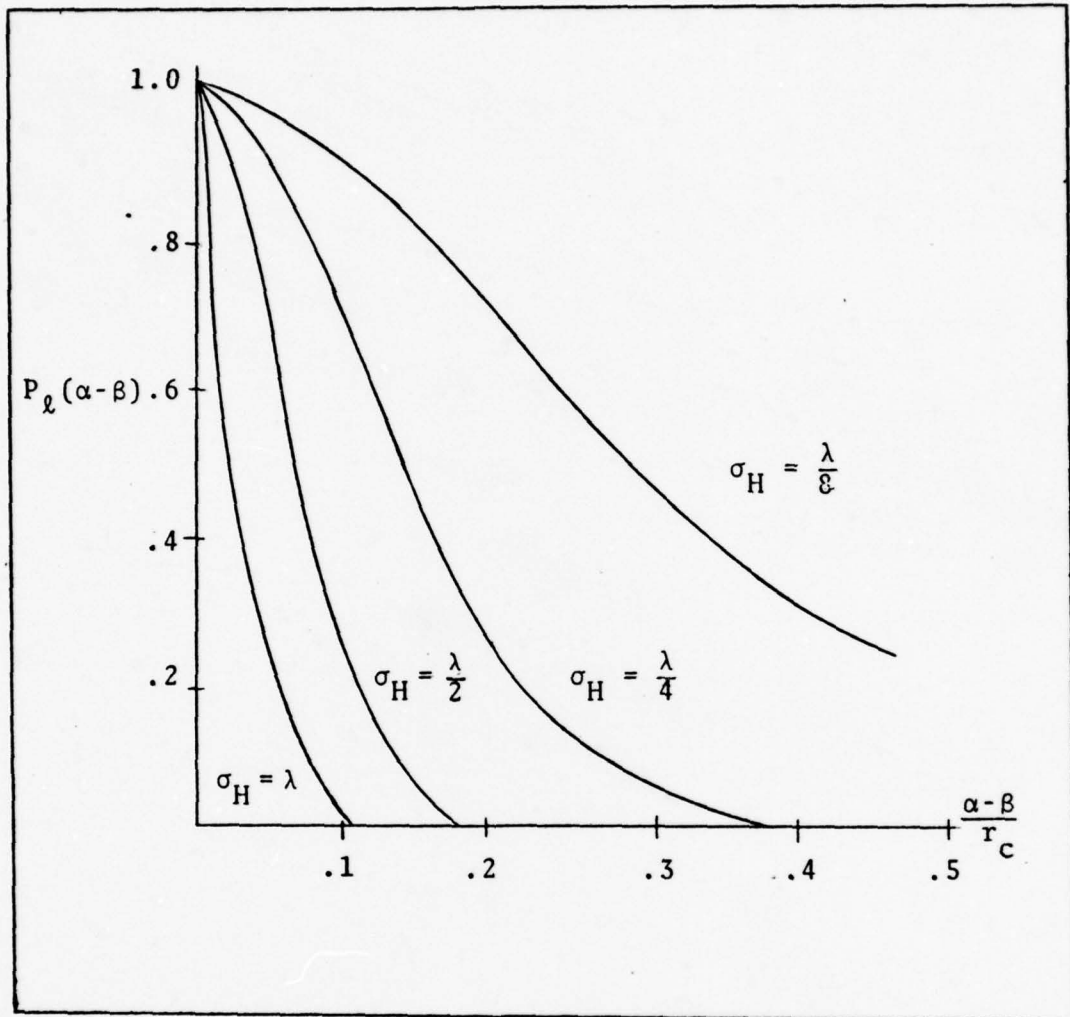


Fig. 4 Plot of  $P_l(\alpha-\beta)$  Ref (16:34)

which can be rewritten as

$$\frac{W(z)}{z} < < \frac{\lambda}{4\pi l} \quad (52)$$

where  $\frac{W(z)}{z}$  is the beam divergence of the laser. The laser can be designed to meet the condition of Eq. (52). For example the beam divergence of a  $1.06\mu\text{m}$  laser must be less than 8 milliradians. Beam divergences are typically less than 1 milliradian, thus the approximation of Eq. (48) holds. Now

the mean of the current becomes

$$E[i_d(t)] = A_1 \int \int P_{DF}(\alpha-\beta) a(\alpha+vt) a(\beta+vt) h(\alpha) h(\beta) P_\rho(\alpha-\beta) d\alpha d\beta \quad (53)$$

Due to the approximation in Eq. (48), the mean of the current is no longer dependent on the quadratic terms in the exponential. Thus, the resulting mean is identical to that obtained in the far field case.

In Eq. (53), only the field correlation function,  $P_\rho(\alpha-\beta)$  and the spatial Fourier transform of the detector surface,  $P_{DF}(\alpha-\beta)$ , are dependent on the argument " $\alpha-\beta$ ". Recall that  $P_\rho(\alpha-\beta)$  was plotted in Fig. 4. For the case of  $\sigma_H = \lambda$ ,  $P_\rho(\alpha-\beta)$  is plotted once more in Fig. 5a. Note that the width of  $P_\rho(\alpha-\beta)$  is only a few micrometers. Generally, the width  $P_{DF}(\alpha-\beta)$  is much wider. For example, assume that the detector surface is of the form in Fig. 5b. It has a width  $D$ , and a uniform transmittance of one. Then

$$P_{DF}(\alpha-\beta) = F_x[P_D(x)] \Big|_{f_x = \frac{\alpha-\beta}{\lambda z}} = \frac{\sin(2\pi \frac{\alpha-\beta}{\lambda z} D)}{\frac{\alpha-\beta}{\lambda z}} \quad (54)$$

$P_{DF}(\alpha-\beta)$  is plotted in Fig. 5c. The width of  $P_{DF}(\alpha-\beta)$  (ignoring the side lobes) is  $\lambda z / D/2$ . For typical values of  $\lambda = 1.06\mu\text{m}$ ,  $z = 10^3$  meters, and  $D = 10$  centimeters, the width of  $P_{DF}(\alpha-\beta)$  is approximately 20 millimeters. Because  $P_{DF}(\alpha-\beta)$  is much wider than  $P_\rho(\alpha-\beta)$ , it is constant over the region where  $P_\rho(\alpha-\beta)$  is non-zero. Thus their effective product is

$$P_{DF}(\alpha-\beta) P_\rho(\alpha-\beta) = P_{DF}(0) P_\rho(\alpha-\beta) \quad (55)$$

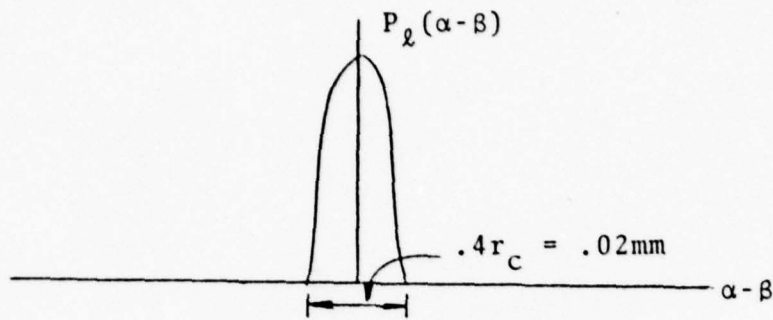


Fig. 5a Field Correlation Function for  $\sigma_H = \lambda$

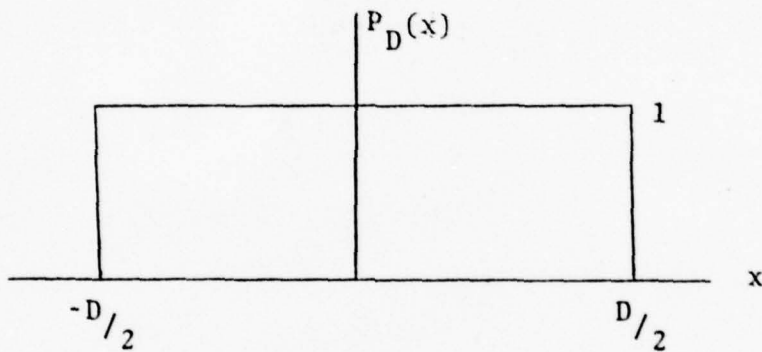


Fig. 5b Detector Aperture Function

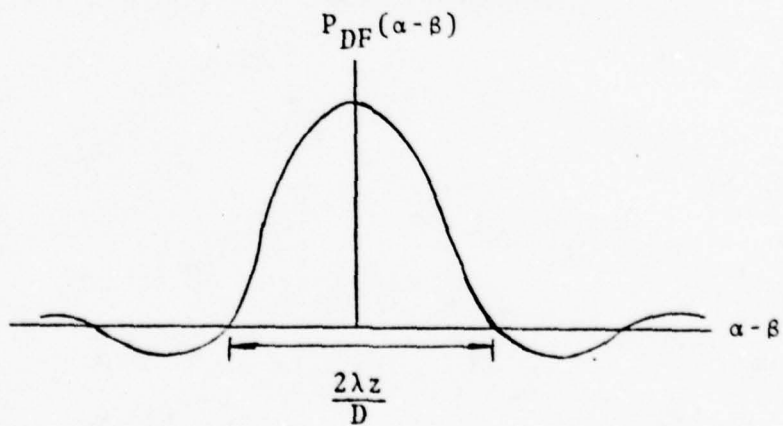


Fig. 5c Fourier Transform of  $P_D(x)$

Fig. 5 Illustration of Function Widths

Eq. (53) now becomes

$$E[i_d(t)] = A_1 P_{DF}(0) \int \int a(\alpha+vt)a(\beta+vt) h(\alpha)h(\beta) P_{\rho}(\alpha-\beta)d\alpha d\beta \quad (56)$$

Using the change of variables,  $x = \alpha + vt$  and  $y = \beta + vt$ , the mean is

$$E[i_d(t)] = A_1 P_{DF}(0) \int \int a(x)a(y) P(x-y) h(x-vt)h(y-vt) dx dy \quad (57)$$

Eq. (57) is the "signal" component in the second moment model for a direct detection receiver. The model will be presented after the covariance of the receiver current, Eq. (37), is found. Eq. (57) is valid for the following conditions: (1) the field incident on the detector is due to the reflection of a monochromatic laser field from a rough surface, (2) the RMS surface roughness is greater than the laser wavelength, (3) the laser is design so that its beam divergence is less than  $\frac{\lambda}{4\pi\ell}$ , and (4)  $P_{DF}(\alpha-\beta)$  is much wider than  $P_{\rho}(\alpha-\beta)$ . Now the covariance will be found.

The Covariance of the Current. In the second moment model, the covariance describes the "noise" or the fluctuation of the current from its mean. It is found by first determining the correlation of the current. From Eqs. (6) and (37)

$$\begin{aligned}
R_{i_d}(t, t') &= E[i_d(t) i_d(t')] \\
&= A_1^2 \int \int \int \int P_{DF}(\alpha - \beta) P_{DF}(\alpha' - \beta') a(\alpha + vt) \\
&\quad a(\beta + vt) a(\alpha' + vt') a(\beta' + vt') h(\alpha) h(\beta) h(\alpha') h(\beta') \\
&\quad E[\exp[j(\theta(\alpha + vt) + \theta(\alpha' + vt') - \theta(\beta + vt) - \theta(\beta' + vt'))]] \\
&\quad d\alpha d\beta d\alpha' d\beta' \quad (59)
\end{aligned}$$

The approximation of Eq. (48) was used in Eq. (59).

The expected value of the phase deviation term in Eq. (59) is determined through the application of the moment factoring theorem. Reed (Ref 23: 194-195) has shown that if  $Z_1$ ,  $Z_2$ ,  $Z_3$ , and  $Z_4$  are zero mean, complex jointly Gaussian random processes, then

$$\begin{aligned}
E[Z_1 Z_2 Z_3^* Z_4^*] &= E[Z_1 Z_3^*] E[Z_2 Z_4^*] \\
&\quad + E[Z_1 Z_4^*] E[Z_2 Z_3^*] \quad (60)
\end{aligned}$$

One problem results when the moment theorem is applied. The  $z_n$  term in the moment theorem corresponds to a  $\exp[j\theta]$  term in Eq. (59). It was argued in the section on the rough surface model, that  $\theta$  is described by a Gaussian distribution. Therefore, the distribution of  $\exp[j\theta]$  is not Gaussian. However, the reflected field is just a complex sum of the fields reflected from each point on the rough surface. It can be shown by the Central Limit Theorem (Ref 17:191) that the reflected field incident on the receiver has a Gaussian distribution. Thus, it is assumed that  $\exp[j\theta]$  takes on a Gaussian distribution as it propagates through the atmosphere.



Therefore, the expected value term in Eq. (59) becomes

$$\begin{aligned}\phi_{\theta}(1) &= E[\exp[j(\theta(\alpha+vt) + \theta(\alpha'+vt') - \theta(\beta+vt) - \theta(\beta'+vt'))]] \\ &= E[\exp[j\theta(\alpha+vt) - j\theta(\beta+vt)]] E[\exp[j\theta(\alpha'+vt') - j\theta(\beta'+vt')]] \\ &\quad + E[\exp[j\theta(\alpha+vt) - j\theta(\beta'+vt')]] E[\exp[j\theta(\alpha'+vt') - j\theta(\beta+vt)]] \quad (61)\end{aligned}$$

The characteristic function can be used to show that

$$\begin{aligned}\phi_{\theta}(1) &= \exp[-\sigma_{\theta}^2(1-\rho(\alpha-\beta))] \exp[-\sigma_{\theta}^2(1-\rho(\alpha'-\beta'))] \\ &\quad + \exp[-\sigma_{\theta}^2(1-\rho(\alpha-\beta'+v\Delta t))] \exp[-\sigma_{\theta}^2(1-\rho(\alpha'-\beta-v\Delta t))] \quad (62)\end{aligned}$$

Recall that the field correlation function was defined in Eq. (47) as

$$P_{\ell}(\alpha) = \exp[-\sigma_{\theta}^2(1-\rho(\alpha))] \quad (63)$$

thus

$$\phi_{\theta}(1) = P_{\ell}(\alpha-\beta)P_{\ell}(\alpha'-\beta') + P_{\ell}(\alpha-\beta'+v\Delta t) P_{\ell}(\alpha'-\beta-v\Delta t) \quad (64)$$

Recall further from Eq. (5) that

$$R_{i_d}(t, t') = E[i_d(t)]E[i_d(t')] + C_{i_d}(t, t') \quad (65)$$

The first term,  $P_{\ell}(\alpha-\beta)P_{\ell}(\alpha'-\beta')$ , in the summation of Eq. (64) corresponds to  $E[i_d(t)]E[i_d(t')]$ . Thus the covariance of the current is

$$C_{i_d}(t, t') = A_1^2 \int \int \int \int a(\alpha+vt)a(\alpha'+vt')a(\beta+vt)a(\beta'+vt')$$

$$h(\alpha)h(\beta)h(\alpha')h(\beta') P_{DF}(\alpha-\beta) P_{DF}(\alpha'-\beta')$$

$$P_\rho(\alpha-\beta'+v\Delta t) P_\rho(\alpha'-\beta-v\Delta t) d\alpha d\beta \quad (66)$$

Eq. (66) is difficult to interpret because the Fourier transform of the aperture is dependent on " $\alpha-\beta$ " and " $\alpha'-\beta'$ " but the field correlation function is dependent on " $\alpha-\beta'$ " and " $\alpha'-\beta$ ". Thus in Eq. (66) the following simplification is made:

$$P_{DF}(\alpha-\beta) \leq P_{DF}(0) \quad (67)$$

and

$$P_{DF}(\alpha'-\beta') \leq P_{DF}(0) \quad (68)$$

This simplification produces an upper bound on the covariance. It is written as

$$C_{i_d}(t, t') \leq A_1^2 \int \int \int \int a(\alpha+vt)a(\beta+vt)a(\alpha'+vt')a(\beta'+vt')$$

$$h(\alpha)h(\beta)h(\alpha')h(\beta') P_{DF}^2(0)$$

$$P_\rho(\alpha-\beta'+v\Delta t) P_\rho(\alpha'-\beta-v\Delta t) d\alpha d\beta d\alpha' d\beta' \quad (69)$$

which is rewritten

$$C_{i_d}(t, t') \leq [A_1 P_{DF}(0) \int \int a(\alpha+vt)a(\beta'+vt')h(\alpha)$$

$$h(\beta') P_\rho(\alpha-\beta'+v\Delta t) d\alpha d\beta']^2 \quad (70)$$

The correlation distance of the current is difficult to determine since the covariance, Eq. (70), is nonstationary.

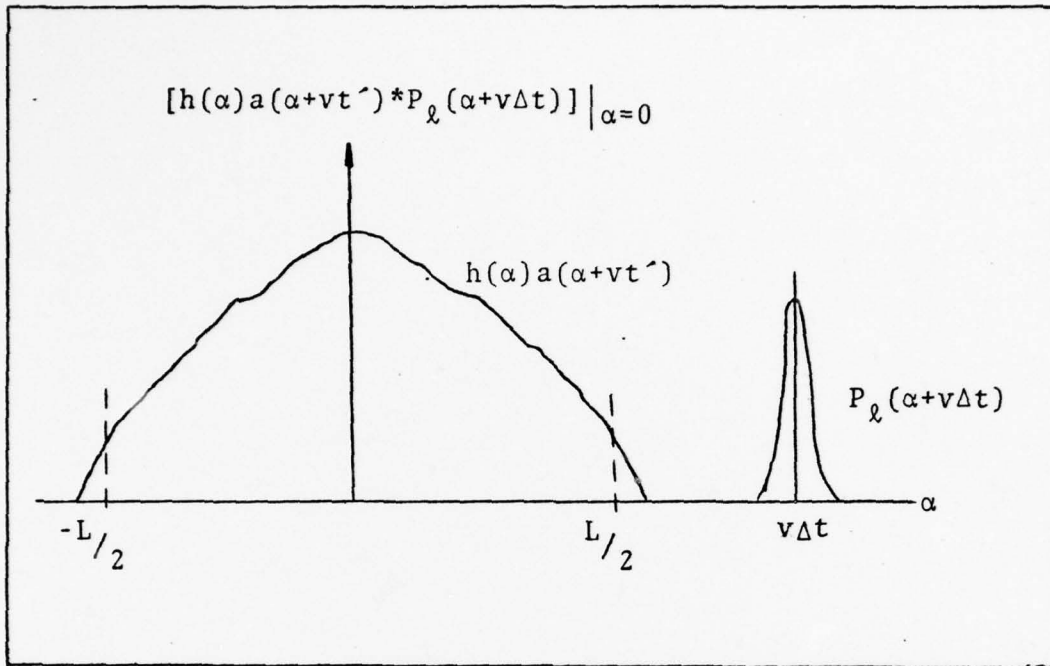


Fig. 6 Graphical Representation of Current Correlation Distance

An idea of the correlation distance can be obtained by writing Eq. (70) as

$$C_{i_d}(t, t') \leq [A_1 P_{DF}(0) \int a(\alpha+vt)h(\alpha) [a(\alpha+vt')h(\alpha) * P_\ell(\alpha+v\Delta t)]d\alpha]^2 \quad (71)$$

where \* denotes the convolution process. The convolution is graphically represented in Fig. 6. The maximum width of  $P_\ell(\alpha+v\Delta t)$  is  $\ell$ , the field correlation distance. The maximum width of  $a(\alpha+vt)h(\alpha)$  and  $a(\alpha+vt')h(\alpha)$  is determined by the beam spot size. This distance is denoted as  $L$ .  $L$  is much greater than  $\ell$ . When  $v\Delta t$  is greater than  $L/2$ , the convolution of  $a(\alpha+vt')h(\alpha)$  with  $P_\ell(\alpha+v\Delta t)$  is equal to zero. Therefore, the maximum correlation distance of the current is

$$L = 2 v \Delta t \quad (72)$$

and the correlation time of the current is

$$\Delta t = \frac{L}{2v} \quad (73)$$

From Eqs. (72) and (73) it is seen that the correlation distance increases with increasing correlation time. It should be noted, that if the reflectance,  $a(\alpha+vt')$ , fluctuates very much within the distance  $L$ , then the correlation distance and time of Eqs. (72) and (73) will become less.

The Direct Detection Model. The direct detection current is modeled using the second moment method. The model is described by the mean and covariance of the current. The mean was given in Eq. (57) as

$$E[i_d(t)] = A_1 P_{DF}(0) \int \int a(\alpha)a(\beta)h(\alpha-vt)h(\beta-vt) P_\rho(\alpha-\beta) d\alpha d\beta \quad (57)$$

It was previously noted that  $P_\rho(\alpha-\beta)$  is very narrow with respect to the other terms in the integral in Eq. (57). Due to its narrowness,  $P_\rho(\alpha-\beta)$  is approximated by the Dirac Delta function,

$$P_\rho(\alpha-\beta) = A_2 \delta(\alpha-\beta) \quad (74)$$

where  $A_2$  is the area of  $P_\rho(\alpha-\beta)$  and is give by

$$A_2 = \int P_\rho(\alpha-\beta) d(\alpha-\beta) \quad (75)$$

Eq. (57) becomes

$$\begin{aligned}
E[i_d(t)] &= A_1 A_2 P_{DF}(0) \int \int a(\alpha) a(\beta) h(\alpha - vt) \\
&\quad h(\beta - vt) \delta(\alpha - \beta) d\alpha d\beta \\
&= A_1 A_2 P_{DF}(0) \int a^2(\alpha) h^2(\alpha - vt) d\alpha
\end{aligned} \tag{76}$$

Recall from Eq. (35) that  $h(\alpha)$  is an even function, thus,

$$\begin{aligned}
E[i_d(t)] &= A_1 A_2 P_{DF}(0) \int a^2(\alpha) h^2(vt - \alpha) d\alpha \\
&= A_1 A_2 P_{DF}(0) [a^2(x) * h^2(x)]
\end{aligned} \tag{77}$$

Eq. (77) implies that the "signal" component of the second moment model is proportional to the convolution of the surface reflection coefficient squared,  $a^2(x)$ , with the system function squared,  $h^2(x)$ .

To complete the second moment model for the direct detection current, the "noise" component is found. Eq. (70) gave the upper bound on the covariance as

$$\begin{aligned}
C_{i_d}(t, t') &\leq [A_1 P_{DF}(0) \int \int a(\alpha) a(\beta) h(\alpha - vt) h(\beta - vt') \\
&\quad P_L(\alpha - \beta) d\alpha d\beta]^2
\end{aligned} \tag{78}$$

This equation describes the "noise" term in the second moment model. The double integral in the above equation is equivalent to the correlation function at the output of a linear filter whose input was a zero mean noise. To see this consider a zero mean noise,  $n(x)$ , input to a linear filter,  $h(x)$ . The filter output is

$$\begin{aligned} n_1(x) &= n(x)*h(x) \\ &= \int n(\alpha)h(x-\alpha)d\alpha \end{aligned} \quad (79)$$

The correlation of the filter output is

$$\begin{aligned} R_{n_1}(x,x') &= E[n_1(x)n_1(x')] \\ &= \int \int E[n(\alpha)n(\beta)]h(x-\alpha)h(x'-\beta)d\alpha d\beta \\ &= \int \int R_n(\alpha\beta)h(x-\alpha)h(x'-\beta)d\alpha d\beta \end{aligned} \quad (80)$$

Comparing Eq. (80) with the double integral in Eq. (78) it is seen the correlation function of the noise is

$$R_n(x,x') = a(x)a(x')P_g(x-x') \quad (81)$$

The square of the integral in Eq. (78) implies that the covariance of the current is equivalent the multiplication of two noise sources. These sources are identically distributed, statistically independent, and have a correlation function given by Eq. (81). The second moment model of the direct detection current is now complete. The model is diagramed in Fig. 7.

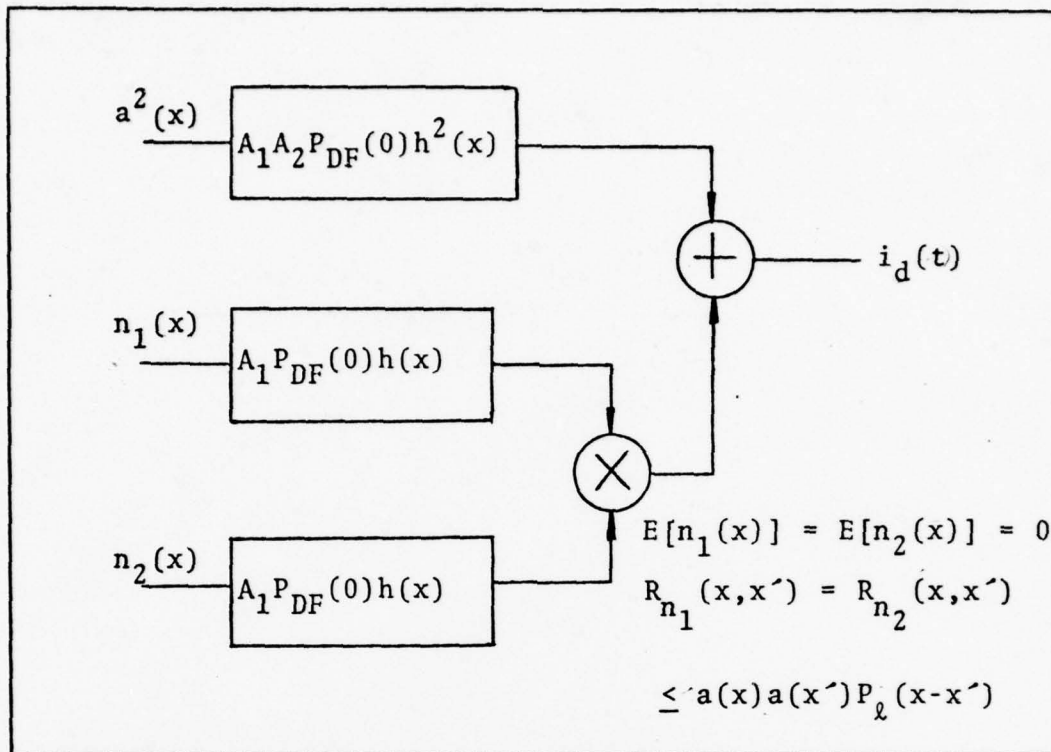


Fig. 7 Direct Detection Current Model

Recall that all noise terms, other than speckle, were neglected. Thus the noise in this model represents speckle noise. The model presented above can easily be modified to include the quantum noise effects that were neglected in the receiver output current.

A parameter that is typically used to measure performance is the signal to noise ratio, denoted SNR. The SNR is defined to be the ratio of signal power to noise power in a system. In statistical terms, the SNR is the mean squared divided by the variance (Ref 24:264). For the direct detection current model, the SNR is

$$\begin{aligned}
\text{SNR}_i &= \frac{E^2[i(t)]}{\sigma_i^2} \\
&= \frac{E^2[i(t)]}{C_{i_d}(t, t'=t)}
\end{aligned}
\tag{82}$$

Substituting Eq. (57) and (70) into Eq. (82) gives the result

$$\text{SNR}_{i_d} \geq 1
\tag{83}$$

The "greater than or equal to" sign occurs because of the upper bound on the covariance.

Several points can be noted about the direct detection current model. The spatial filtering effects of  $h^2(x)$  are seen by taking the spatial Fourier transform of  $E[i_d(t)]$  as given in Eq. (77).

$$F_x[E[i_d(t)]] = A_1 A_2 P_{DF}(0) A'(f_x) [H'(f_x) * H'(f_x)]
\tag{84}$$

where  $A'(f_x) = F_x[a^2(x)]$  and  $H'(f_x) = F_x[h(x)]$ .

The Fourier transform has an inverse effect on the width of a function. That is, as  $h(x)$  gets wider  $H'(f_x)$  and thus the convolution of  $H'(f_x)$  with itself gets narrower. The results is that as the system function gets wider in space, it blocks out the high spatial frequency content of  $a^2(x)$ .

The model for  $E[i_d(t)]$  is identical to the result discussed by Goodman for an incoherent imaging system (Ref 13:109).



Thus the direct detection current model can be thought of as an incoherent imaging system with an additive noise term.

Last of all, it can be seen from either Eq. (78) or Fig. 7 that the noise is signal dependent. Thus as the signal,  $a^2(x)$ , increases or decreases, the noise also increases or decreases by a proportional amount. Thus the SNR can not be improved by increasing the signal power. This is in contrast to many other noise models which are signal independent.

This concludes the discussion of the direct detection current model. The current model for the heterodyne receiver is determined in the following section.

#### The Heterodyne Receiver Current Model

A second moment model for the receiver current of a monochromatic laser-heterodyne receiver system has been determined by Lyons (Ref 16:46). The procedure used to establish the heterodyne current model is very similar to that used to find the direct detection current model of this thesis. Lyons' results are presented below.

The heterodyne receiver current is (Ref 16:31)

$$i_h(t) = A_3 \int a(\alpha+vt)h(\alpha)\exp[j\theta(\alpha+vt)]\exp[-j\frac{k\alpha^2}{z}]P_{DF}(\alpha)d\alpha \quad (85)$$

where  $A_3 = \frac{2q\eta A}{hf_0\lambda z}$  and  $a(\alpha)$ ,  $h(\alpha)$ ,  $\theta(\alpha)$ , and  $P_{DF}(\alpha)$  are the same as defined for the direct detection current. Due to the defining equation (Ref Eq. (4)) for the heterodyne receiver current, the current of Eq. (86) is centered at the optical frequency  $f_0 - f_{IF}$ . Also, this current is complex in contrast

to the direct detection current which is real (Ref Eq. (34)).  
The expected value of the heterodyne current is (Ref 16:31)

$$E[i_h(t)] = 0 \quad (86)$$

and its covariance is (Ref 16:36)

$$C_{i_h}(t, t') = A_3^2 \int \int P_{DF}(\alpha) P_{DF}(\alpha') a(\alpha+vt) a(\alpha'+vt') h(\alpha) h(\alpha') P_\rho(\alpha'+v\Delta t) d\alpha d\alpha' \quad (87)$$

where  $P_\rho(\Delta\alpha)$  is given by Eq. (47) and  $\Delta\alpha = \alpha - \alpha'$ .

The heterodyne current is centered at the frequency  $f_o - f_{IF}$ . Thus even though its mean is equal to zero, this does not imply that the mean of the amplitude of the current is zero. The current amplitude, denoted  $A(t)$ , is found by writing the current as the sum of its real and imaginary parts. It is

$$\begin{aligned} i_h(t) &= I_r + j I_i \\ &= A(t) \cos \gamma(t) + j A(t) \sin \gamma(t) \end{aligned} \quad (88)$$

In polar form this becomes

$$i_h(t) = A(t) e^{j\gamma(t)} \quad (89)$$

The current is physically broken into its real and imaginary parts by the well known quadrature model (Ref 24:238) as shown in Fig. 8a. Note that the quadrature outputs are the real and imaginary parts of the currents. If the quadrature outputs are squared and then added together, the resulting output is the current amplitude squared,  $A^2(t)$ , as shown in Fig. 8b.

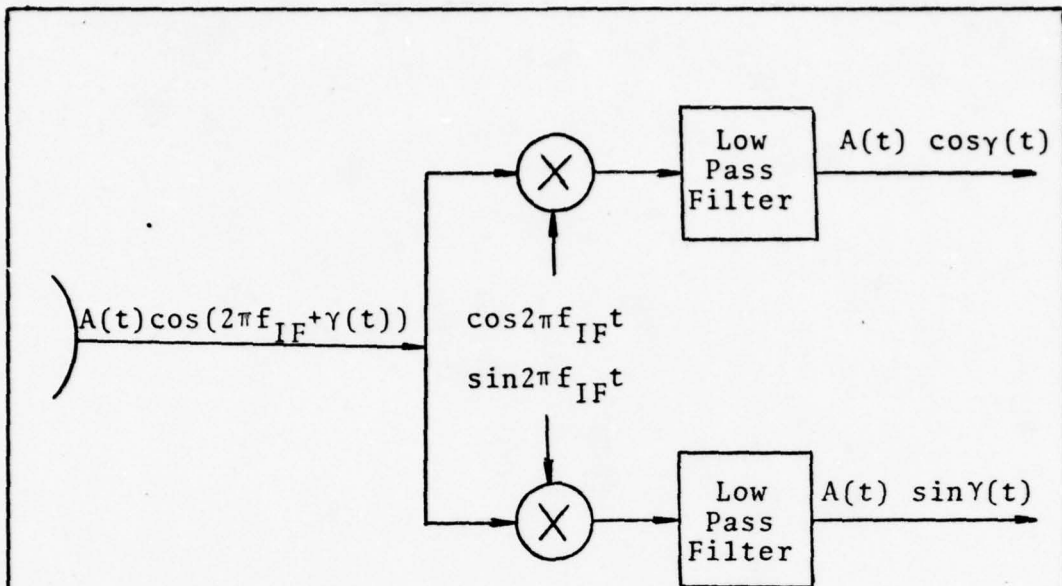


Fig. 8a The Quadrature Model (Ref 16:40)

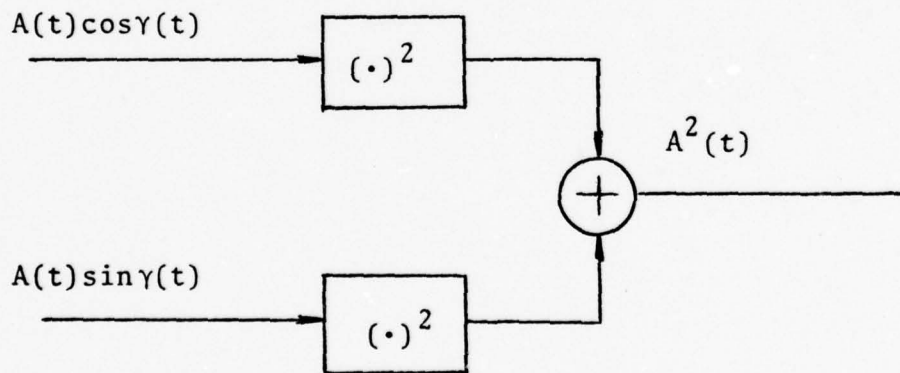


Fig. 8b Determination of  $A^2(t)$  from the Quadrature Outputs (Ref 16:43)

Fig. 8 Determination of  $A^2(t)$ .

The mean (Ref 16:43) and the covariance (Ref 16:45) of  $A^2(t)$  are

$$E[A^2(t)] = C_i(t, t' = t) \quad (90)$$

and

$$C_{A^2}(t, t') = [C_i(t, t')]^2 \quad (91)$$

By substituting Eq. (87) into Eq. (90), the mean of  $A^2(t)$  is expressed in terms of the reflectance,  $a(\alpha)$ , and the system function,  $h(\alpha)$  as follows:

$$E[A^2(t)] = A_3^2 \int \int h(\alpha)h(\alpha')P_{DF}(\alpha)P_{DF}(\alpha')a(\alpha+vt)a(\alpha'+vt)P_\rho(\Delta\alpha)d\alpha d\alpha' \quad (92)$$

As in Eq. (74),  $P_\rho(\Delta\alpha)$  can be approximated by the Dirac Delta function

$$P_\rho(\Delta\alpha) = A_4\delta(\Delta\alpha) \quad (93)$$

where  $A_4$  is the area of  $P_\rho(\Delta\alpha)$  which is given by

$$A_4 = \int P_\rho(\Delta\alpha) d\Delta\alpha \quad (94)$$

Eq. (92) then becomes

$$E[A^2(t)] = A_3^2 A_4 \int h^2(\alpha)P_{DF}^2(\alpha)a^2(vt-\alpha) d\alpha \quad (95)$$

which by a change of variables is written

$$E[A^2(t)] = A_3^2 A_4 \int a(x^2)h^2(vt-x)P_{DF}^2(vt-x)dx \quad (96)$$

Thus the mean of  $A^2(t)$  can be represented by a linear system model of  $a^2(x)$  convolved with  $h^2(x)P_{DF}^2(x)$ .

The covariance of  $A^2(t)$  is found by substituting Eq. (87) into Eq. (91). It is

$$C_{A^2}(t, t') = [A_3^2 \int \int h(vt-x)h(vt'-x)a(x)a(x') P_{\rho}(x-x')P_{DF}(vt-x)P_{DF}(vt'-x')dx dx']^2 \quad (97)$$

Thus as in the direct detection case, the double integral in the above equation is identical to the output correlation of a filter,  $h(x)$ , whose input is a zero mean noise process with the correlation function

$$R_n(x, x') = a(x)a(x')P_{\rho}(x-x') \quad (98)$$

Once again the square of the integral simply means that the noise can be represented by the product of two identically distributed, statistically independent noise processes. The second moment model for the amplitude squared of the heterodyne receiver current is shown in Fig. 9. As with the direct detection current model, this model can easily be modified to include quantum noise effects. These noise terms are included by simply adding them to the speckle noise term described by Eq. (97).

The SNR for the heterodyne current model is found by substituting Eqs. (92) and (97) into Eq. (82). The Resulting SNR is

$$SNR_{i_h} = 1 \quad (99)$$

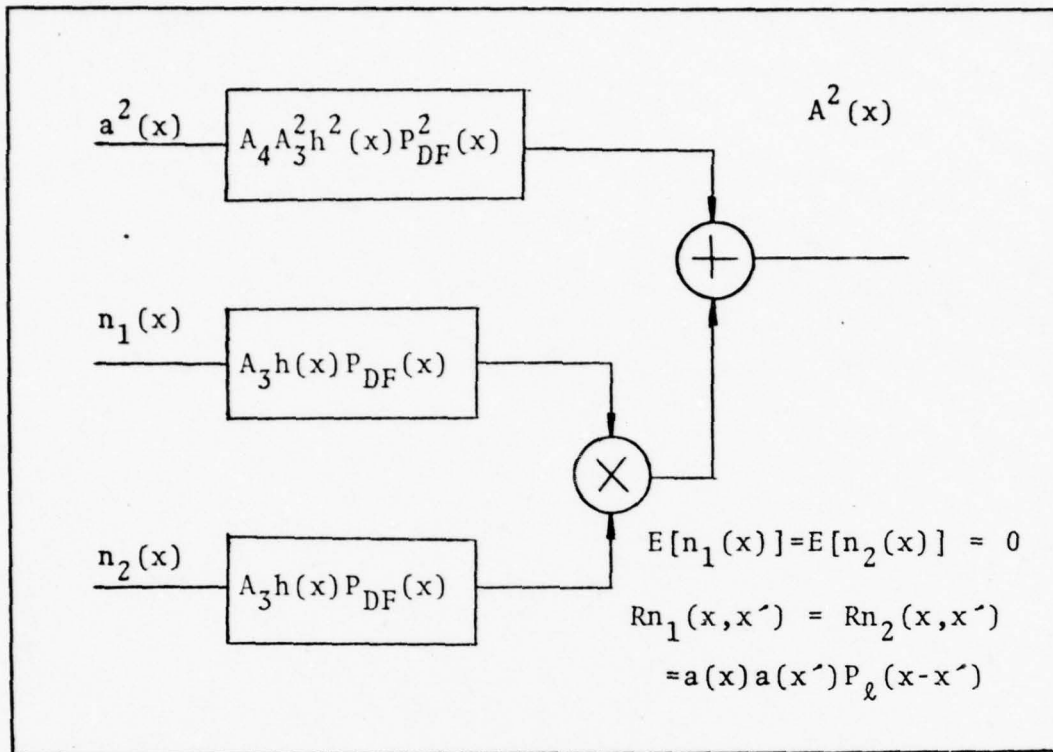


Fig.9 The Model for the Amplitude Squared of the Heterodyne Receiver Current (Ref 16:46)

The model for the amplitude squared of the heterodyne current and the direct detection current model are very similar. The only differences are: (1) the covariance of the heterodyne current model has a specific value rather than a bound, (2) the system function of the heterodyne current model is dependent on both  $h(x)$  and  $P_{DF}(x)$ , and (3) the two models differ depending on the constants  $A_1$ ,  $A_2$ ,  $A_3$ , and  $A_4$ . Since there are no major differences in the two models, the comments made about the direct detection model are valid for the heterodyne model. Thus, as the heterodyne system function,  $h'(x) = h(x)P_{DF}(x)$ , becomes wider in space, the higher spatial frequency content

of  $a^2(x)$  is lost and the worse the resolution ability of the system becomes. The model of  $E[A^2(t)]$  is also identical to the result discussed by Goodman (Ref 13:107) for an incoherent imaging system. Thus, square law detection can also be thought of as an incoherent imaging system with an additive noise term. Finally, the noise in the heterodyne model is also signal dependent. Thus the SNR can not be improved by increasing the signal power.

One important result in the comparison the two models is that the SNR for the direct detection model is always equal to or larger than the SNR of the heterodyne model. Therefore at its worst, the direct detection model performs as well as the heterodyne model. Thus on the basis of the SNR, the direct detection receiver produces the better results for the laser line-scan imaging system. However, the SNR is only one of many parameters used to evaluate system performance and should be considered as only a part of the whole picture.

#### IV. The System Models for Quasimonochromatic and Broadband Laser Sources

In Chapter III, the system models for a monochromatic laser were determined. These models are now extended to find the resulting models for broadband and quasimonochromatic sources. First, the monochromatic laser field is extended to broader bandwidths. Then, by using the new laser sources and following the procedure used to determine the previous models, the current models for extended laser sources are found.

##### Quasimonochromatic and Broadband Fields

The laser field given in Eq. (23) is valid for monochromatic lasers only. This field can be modified, so that it is valid for both quasimonochromatic and broadband lasers, by a method known as linear frequency modulation or chirping. The theory of chirping is discussed in a paper by Klauder, et. al. (Ref 25). The following paragraph is a brief summary of the results of chirping.

Consider a rectangular time pulse with width T seconds and denoted  $\text{rect}[t/T]$ . The bandwidth of this pulse is found, by Fourier analysis, to be approximately  $\frac{1}{T}$  Hz. If this pulse is chirped, its resulting waveform, denoted  $U_0(t)$ , is (Ref 25:754)

$$U_0(t) = \text{rect}[t/T] \exp[j\pi\Delta f t^2] \quad (100)$$

where  $\exp[j\pi\Delta f t^2]$  is the chirp waveform and  $\Delta f$ , whose value is chosen by the system design, has units of inverse seconds squared. It is shown (Ref 25: 755-758) by Fourier analysis



and Fresnel integral techniques, that if the product  $\Delta f T^2$  is greater than or equal to ten, the bandwidth of  $U_0(t)$  is  $\Delta f T$ . The significance of this result is seen in the following example. Suppose a rectangular pulse has a width of 10msec and thus a bandwidth of 100Hz. Assume that  $\Delta f = 10^5 \text{ (sec)}^{-2}$  by system design. Therefore  $\Delta f T^2 = 10$  which implies that  $U_0(t)$  has a bandwidth of  $\Delta f T = 1 \text{ KHz}$ . Thus the bandwidth of a signal has been extended by an order of magnitude by chirping. If  $\Delta f$  were chosen to be  $10^6 \text{ (sec)}^{-2}$ , the bandwidth would have increased by two orders of magnitude. The point here is that a wave of any desired bandwidth can be produced by chirping.

This point also holds for the monochromatic laser field in Eq. (23). Eq. (23) is spatially dependent only. Thus when pictured in time, it has a constant amplitude and extends for all time. Ideally it could be thought of as a rectangular time pulse with infinite width. However, in reality the width is only the time interval for which the laser is turned on. In the laser line-scan imaging system, this interval could be thought of as the time needed to make a single scan of the object surface. In any case, multiplying Eq. (23) by the chirp waveform results in a field which is not monochromatic, but rather it has some bandwidth. This bandwidth is determined by  $\Delta f$  and the time interval for which the laser is on. It is reasonable to assume that the chirped laser field can be designed to be either quasimonochromatic or broadband. In either case, the general form of the chirped laser field is

$$U(\alpha, t) = \frac{A}{(\lambda z)^{\frac{1}{2}}} \exp[j(kz - \frac{\pi}{4})] \exp[j\frac{k}{2z}\alpha^2] \exp[-\frac{\alpha^2}{W^2(z)}] \exp[j\pi\Delta f t^2] \quad (101)$$

With the use of this chirped field, it is possible to determine the system models for the extended bandwidth sources.

### The Quasimonochromatic System Models

A quasimonochromatic laser source is used with both a direct detection and a heterodyne receiver. The second moment models for the two systems are determined. First, the reflected laser field that is incident on the detector surface is found.

#### The Quasimonochromatic Field Incident on the Detector.

Quasimonochromatic fields are defined in Appendix A as those which suffered a negligible time delay during propagating. Thus quasimonochromatic fields are similar to monochromatic ones in that they both propagate independent of time. For the quasimonochromatic case the field at the detector is given by Eqs. (18) and (21):

$$U_d(x, t) = \frac{1}{(\lambda z)^{\frac{1}{2}}} \exp[-j(kz - \frac{\pi}{4})] \exp[-jk\frac{x^2}{2z}] \int U_{r,Q}(\alpha, t) \exp[-j\frac{k}{2z}\alpha^2] \exp[j2\pi\frac{x\alpha}{\lambda z}] d\alpha \quad (102)$$

where

$$U_{r,Q}(\alpha, t) = a(\alpha+vt) \exp[j\theta(\alpha+vt)] \frac{A}{(\lambda z)^{\frac{1}{2}}} \exp[-\frac{\alpha^2}{W^2(z)}] \exp[j(kz - \frac{\pi}{4})] \exp[-j\frac{k}{2z}\alpha^2] \exp[-j\pi\Delta f t^2] \quad (103)$$

Substituting Eq. (103) into Eq. (102), the field at the detector is

$$U_d(x,t) = \frac{A}{\lambda z} \exp[-j2(kz - \frac{\pi}{4})] \exp[-jk\frac{x^2}{2z}] \exp[-j\pi\Delta f t^2] \\ \int a(\alpha+vt) \exp[j\theta(\alpha+vt)] h(\alpha) \exp[-j\frac{k}{z}\alpha^2] \\ \exp[j2\frac{x\alpha}{\lambda z}] d\alpha \quad (104)$$

Note that except for the chirp term, Eq. (104) is identical to the field incident on the detector for the monochromatic case (Ref Eq. (28)). Eq. (104) is now used to determine the direct detection model.

#### The Quasimonochromatic-Direct Detection Current Model.

The ideal direct detection receiver current is given by Eq. (5) as

$$i_d(t) = \frac{q\eta}{hf_0} \iint |U_d(x,y)|^2 dx dy \quad (5)$$

In Eq. (5), the current is proportional to the magnitude of the field incident on the detector surface. Taking the magnitude of Eq. (104) cancels the chirp term with its conjugate. Thus the magnitude of the field incident on the detector is the same for both the monochromatic and quasimonochromatic laser sources. The result is that the second moment models for the direct detection current are identical in both cases.

This finding is not a complete surprise. From Eq. (20) and for a typical value of  $|\tilde{r}_{01}|_{\max} = 10^3$  meters, the quasimonochromatic field must have a bandwidth much less than  $3 \times 10^5$  Hz. Thus with respect to the laser frequency, the

quasimonochromatic field is almost monochromatic and the two direct detection current models should be similar. In this thesis it has been assumed that lasers can be monochromatic, when in reality those lasers referred to as monochromatic actually have some narrow bandwidth. The above results shows that assumption of modeling a narrowband source as monochromatic is valid. Finally, since both direct detection current models are identical, they have the same SNR and resolution characteristics. The heterodyne current model is now investigated.

The Quasimonochromatic-Heterodyne Current Model. The ideal current of the heterodyne receiver is given by Eq. (4) as

$$i_h(t) = \frac{2qn}{hf_0} \int \int_{A_d} \text{Re}\{U_d(x,y)U_{LO}^*(x,y)\exp[-j2\pi f_{IF}t]\} dx dy \quad (4)$$

Substituting Eq. (104) into Eq. (4), the current is

$$i_{h,Q}(t) = A_3 \text{Re}\{\exp[-j2(kz - \frac{\pi}{4})]\exp[-j\pi\Delta f t^2]\exp[-j2\pi f_{IF}t] \\ \int \int P_D(x) a(\alpha+vt) h(\alpha) \exp[j\theta(\alpha+vt)] \exp[-j\frac{k}{2}\alpha^2] \\ \exp[-j\frac{k}{2z}x^2] U_{LO}^*(x,t) \exp[j2\pi\frac{x\alpha}{\lambda z}] d\alpha dx\} \quad (105)$$

In the above equation, the  $\exp[-j\pi\Delta f t^2]$  and  $\exp[-j\frac{k}{2z}x^2]$  terms can be cancelled by identical phase terms in the local oscillator. The  $x$  integral is now the spatial Fourier transform of the aperture function denoted

$$F_x[P_D(x)] \Big|_{f_x = \frac{\alpha}{\lambda z}} = P_{DF}(\alpha) \quad (106)$$

Only the amplitude of the current is of interest, thus the phase terms in front of the integral are neglected. Also,  $\exp[-j \frac{k\alpha^2}{z}] \cong 1$  as shown in the approximation of Eq. (48). The current is now written as

$$i_{h,Q}(t) = A_3 \int P_{DF}(\alpha) a(\alpha+vt) h(\alpha) \exp[j\theta(\alpha+vt)] d\alpha \quad (107)$$

This result is identical to the complex current of Eq. (85). Thus as resulted for direct detection current models, the heterodyne current models are identical for the monochromatic and quasimonochromatic laser sources. The comments made at the end of the previous section for the direct detection current models could also be stated for the heterodyne current models.

#### The Broadband System Models

The second moment models are found for two systems: a broadband laser-heterodyne receiver and a broadband laser-direct detection receiver system. The laser field is assumed to be broadband due to an appropriate chirp term. First, the field incident on the detector is determined.

The Broadband Field Incident on the Detector. A broadband field was defined in Appendix A as one which suffers a time delay during propagation. Because of this delay, the mathematics involved in propagating a broadband field are somewhat more difficult than for a monochromatic or quasimonochromatic field. The configuration for determining the broadband field is illustrated in Fig. 10.

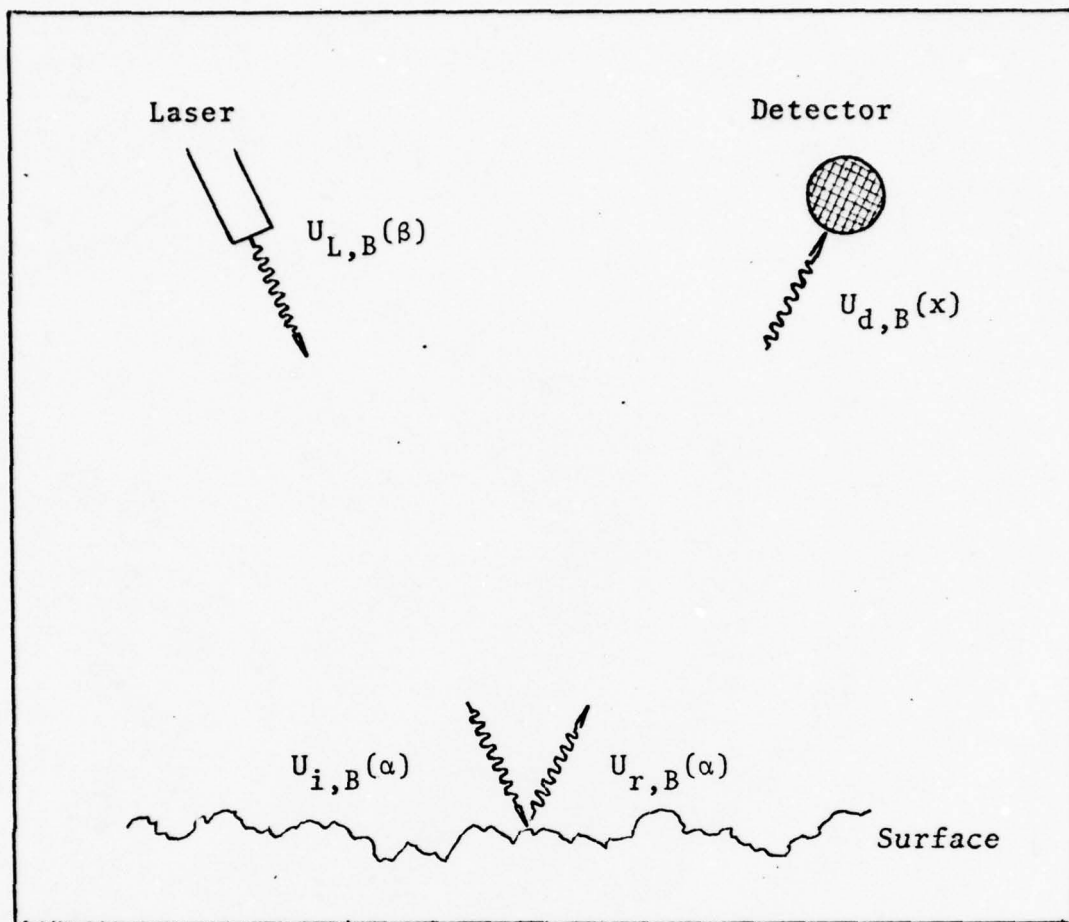


Fig. 10 Notation for the Broadband System

Consider the setup of Fig. 10. The monochromatic field at the laser output is given by Siegman as (Ref 15:307)

$$U_L(\beta) = A \exp[-\beta^2/W_0^2] \quad (108)$$

where  $W_0$  is the spot size of the laser beam at the laser output. The broadband laser field at the laser output, denoted  $U_{L,B}(\beta)$  is

$$U_{L,B}(\beta) = A \exp[-\beta^2/W_0^2] \exp[j\pi\Delta f t^2] \quad (109)$$

The broadband field incident on the rough surface, denoted  $U_{i,B}(\alpha)$ , is found by propagating the laser field by the extended Huygens-Fresnel integral given in Eq. (18). The incident field is

$$U_{i,B}(\alpha) = \frac{A}{(\lambda z)^{\frac{1}{2}}} \exp[j(kz - \frac{\pi}{4})] \exp[jk\frac{\alpha^2}{2z}] \int \exp[-\frac{\beta^2}{W_0^2}] \exp[j\pi\Delta f(t - \frac{r_{o1}}{c})^2] \exp[j\frac{k\beta^2}{2z}] \exp[-j\frac{2\pi\alpha\beta}{\lambda z}] d\alpha \quad (110)$$

where  $\frac{r_{o1}}{c}$  is the propagation time delay from the laser to the surface. The field reflected from a rough surface was given in Eq. (25). The reflected broadband field is

$$U_{r,B}(\alpha, t) = a(\alpha + vt) \exp[j\theta(\alpha + vt)] U_{i,B}^*(\alpha, t) \quad (111)$$

The field incident on the detector is determined once again using the extended Huygens-Fresnel integral. It is

$$U_{d,B}(x, t) = \frac{1}{(\lambda z)^{\frac{1}{2}}} \exp[j(kz - \frac{\pi}{4})] \exp[-j\frac{kx^2}{2z}] \int U_r(\alpha, t - \frac{r_{o1}}{c}) \exp[-j\frac{k\alpha^2}{2z}] \exp[j\frac{2\pi\alpha x}{\lambda z}] d\alpha \quad (112)$$

where  $r_{o1}$  is the propagation time delay from the surface to the detector. Substituting Eqs. (110) and (111) into Eq. (112) yields

$$\begin{aligned}
U_{d,B} = & \frac{A}{\lambda z} \exp[j(kz - \frac{\pi}{4})] \exp[-jk \frac{x^2}{2z}] \iint a(\alpha + vt) \exp[j\theta(\alpha + vt)] \\
& \exp[-j \frac{k\alpha^2}{z}] \exp[-\frac{\beta^2}{W_0}] \exp(-j \frac{k\beta^2}{2z}) \exp[j \frac{2\pi}{\lambda z} (\alpha\beta + x\alpha)] \\
& \exp[-j\pi\Delta f(t - \frac{r_{o1}}{c} - \frac{r'_{o1}}{c})^2] d\alpha d\beta \quad (113)
\end{aligned}$$

From Fig. 2 and the approximation of Eq. (11) it is seen that

$$r_{o1} = [z^2 + (\alpha - \beta)^2]^{\frac{1}{2}} \cong z + \frac{1}{2z} (\alpha - \beta)^2 \quad (114)$$

and

$$r'_{o1} = [z^2 + (x - \alpha)^2]^{\frac{1}{2}} \cong z + \frac{1}{2z} (x - \alpha)^2 \quad (115)$$

By use of the last two equations, it can be shown that the exponent in the chirp term is

$$\begin{aligned}
j\pi\Delta f(t - \frac{r_{o1}}{c} - \frac{r'_{o1}}{c})^2 = & j\pi\Delta f[d_1(t) + d_2(t)\{(\alpha - \beta)^2 + (x - \alpha)^2\}] \\
& + \frac{1}{2z^2 c^2} (\alpha - \beta)^2 (x - \alpha)^2 \quad (116)
\end{aligned}$$

where

$$d_1(t) = t^2 + \frac{4z^2}{c^2} - \frac{4tz}{c} \quad (117)$$

and

$$d_2(t) = \frac{2}{c^2} - \frac{t}{cz} \quad (118)$$



The last term in Eq. (116) corresponds to the third term in the binomial expansion given in Eq. (11). Thus it can be neglected. After combining Eq. (116) with Eq. (113), the field at the detector is

$$\begin{aligned}
 U_{d,B}(x,t) = & \frac{A}{\lambda z} \exp[-j2(kz - \frac{\pi}{4})] \exp[-jk\frac{x^2}{2z}] \exp[-j\pi\Delta f d_1(t)] \\
 & \int \int a(\alpha+vt) \exp[j\theta(\alpha+vt)] \exp[-j\frac{k\alpha^2}{2z}] \exp[-j\frac{k\beta^2}{2z}] \\
 & \exp[-\frac{\beta^2}{W_0}] \exp[j\frac{2\pi}{\lambda z}(\alpha\beta+x\alpha)] \\
 & \exp[-j\Delta f\pi d_2(t) \{(\alpha-\beta)^2 + (x-\alpha)^2\}] \, d\alpha d\beta \quad (119)
 \end{aligned}$$

The double integral in the above equation, denoted Q, can be written

$$Q = \int \int g_1(\alpha,\beta) \exp[j\Delta f g_2(\alpha,\beta)] \, d\alpha d\beta \quad (120)$$

where

$$\begin{aligned}
 g_1(\alpha,\beta) = & a(\alpha+vt) \exp[j\theta(\alpha+vt)] \exp[-j\frac{k\alpha^2}{2z}] \\
 & \exp[-j\frac{k\beta^2}{2z}] \exp[-\frac{\beta^2}{W_0}] \exp[j\frac{2\pi}{\lambda z}(\alpha\beta+x\alpha)] \quad (121)
 \end{aligned}$$

and

$$g_2(\alpha,\beta) = -\pi d_2(t) [(\alpha-\beta)^2 + (x-\alpha)^2] \quad (122)$$

Eq. (120) has the form of an integral which can be solved by the method of stationary phase. This method is discussed in Appendix B and can be used to show that as the quantity  $\Delta f$  becomes large,  $Q$  can be approximated by

$$Q \approx [-j\Delta f d_2(t)]^{-1} a(x+vt) \exp[j\theta(x+vt)] \exp[j\frac{kx^2}{2z}] \exp[-\frac{x^2}{w_0^2}] \quad (123)$$

It is emphasized that Eq. (123) is only an approximation which becomes more exact as  $\Delta f$  becomes larger. No attempt is made in this paper to determine the relationship between  $\Delta f$  and the variation of  $Q$  from its actual value. However, this relationship has been analyzed by Cook and Bernfeld (Ref 27: Chapter 3) and by Fowle (Ref 28: 61-67) for integrals similar to Eq. (120). Thus it seems feasible that Eq. (123) can be quantified by an analysis similar to the methods of above two references.

Substituting Eq. (123) into Eq. (119) yields the field incident on the detector which is

$$U_{d,B}(x,t) = \frac{\lambda f_0^2}{\Delta f(2z-tc)} \exp[-j2kz] \exp[-j\pi\Delta f d_1(t)] a(x+vt) \exp[j\theta(x+vt)] \exp[-\frac{x^2}{w_0^2}] \quad (124)$$

This equation is now used to determine the receiver currents.

The Broadband Direct Detection Current Model. The ideal direct detection receiver current is given by Eq. (5). Combining Eq. (5) with Eq. (124) produces a broadband current of

$$i_{d,B}(t) = A_4 \int a^2(x) h_o(vt - x) dx \quad (125)$$

where

$$A_4 = \frac{qn}{hf_o} \left[ \frac{A\lambda f_o^2}{\Delta f(2z-tc)} \right]^2 \quad (126)$$

and

$$h_o(x) = \exp\left[-\frac{2x^2}{W_o}\right] P_D(x) \quad (127)$$

$h_o(x)$ , like  $h(x)$ , is also called the system function.

Note that the broadband current of Eq. (125) contains no random terms. This is an amazing fact because it implies that there is no speckle noise present in the current. Most laser line-scan imaging systems are limited by speckle noise. In fact, the four systems previously investigated in this paper had signal dependent noise. This is obviously not the case for this system since it has no speckle noise. Thus from the above results, it appears that a laser line-scan imaging system which is not speckle noise limited can be designed.

Eq. (125) has the form of a convolution process of  $a^2(x)$  with  $h_o(x)$ . Fig. 11 is a diagram of this model. The quantum noise effects, which were neglected, can be included by adding the appropriate noise terms to the broadband current,  $i_{d,B}(t)$ .

The new system function,  $h_o(x)$ , is dependent on the size of the detector surface and the beam spot size at the laser output,  $W_o$ . It serves the same purpose as the previous system function,

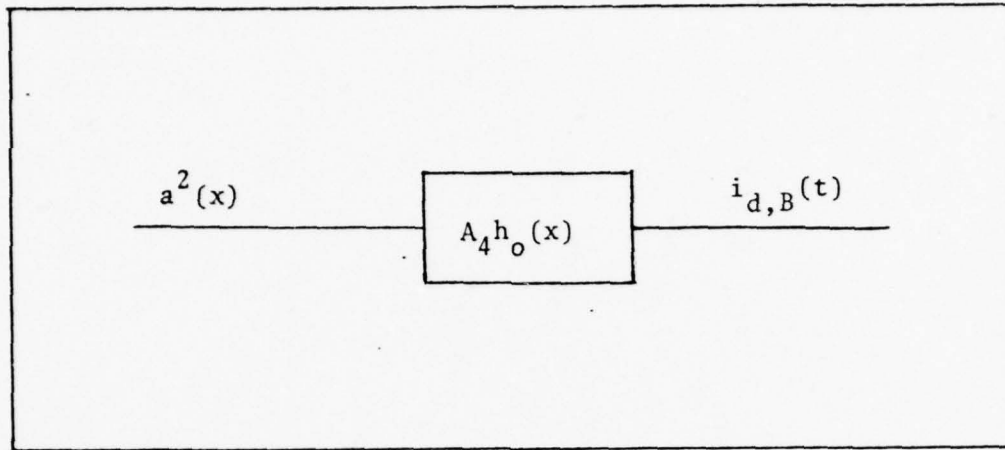


Fig. 11 Broadband-Direct Detection Current Model

$h(x)$ . It was shown in Eq. (84) that as  $h(x)$  becomes wider, the system's resolution ability becomes worse. This comment is true for  $h_o(x)$  also.

The Broadband-Heterodyne Current Model. The broadband heterodyne current is found by substituting Eq. (124) into Eq. (4). The latter equation gives the heterodyne receiver output current which becomes

$$i_{h,B}(t) = A_5 \operatorname{Re}\{\exp[-j2kz] \exp[-j\pi\Delta f d_1(t)] \exp[-j2\pi f_{IF} t] \int a(x+vt) \exp[j\theta(x+vt)] P_D(x) \exp[-\frac{x^2}{2W_o}] U_{LO}^*(x,t) dx\} \quad (128)$$

where

$$A_5 = \frac{2q\eta}{h\nu_0} \frac{A\lambda f_0^2}{F(2z-tc)} \quad (129)$$

In Eq. (128), the  $\exp[-j\pi\Delta f d_1(t)]$  can be cancelled by an identical term in the local oscillator field. Only the current amplitude is of interest, thus the phase terms in front of the integral can be neglected. The complex current is now written as

$$i_{h,B}(t) = A_5 \int P_D(x) a(x+vt) \exp[j\theta(x+vt)] \exp\left[-\frac{x^2}{W_0^2}\right] dx \quad (130)$$

The rough surface phase term is the only random term in Eq. (130). Thus the mean of the current is given by

$$E[i_{h,B}(t)] = A_5 \exp\left[-\frac{\sigma_\theta^2}{2}\right] \int P_D(x) a(x+vt) \exp\left[-\frac{x^2}{W_0^2}\right] dx \quad (131)$$

where  $\exp\left[-\frac{\sigma_\theta^2}{2}\right]$  is the value of the characteristic function from Eq. (41). For a surface with  $\sigma_h \geq \lambda$  in Eq. (28), the value of the characteristic function is approximately zero (Ref. 16:31). Thus the mean of the current is effectively equal to zero;

$$E[i_{h,B}(t)] = 0 \quad (132)$$

The covariance of the current is

$$E[i_{h,B}(t) i_{h,B}(t')] = A_5^2 \iint P_D(x) P_D(x') a(x+vt) a(x'+vt') h_1(x) h_1(x') P_g(\Delta x+v\Delta t) dx dx' \quad (133)$$

where  $h_1(x) = \exp[-\frac{x^2}{w_0^2}]$ . Because of the zero mean, the

correlation of the current is equal to the covariance.

Comparing Eqs. (131) and (132) to Eqs. (86) and (87) reveals that the broadband heterodyne current model is almost identical to the monochromatic model. The only differences in the two are their amplitudes and their system functions. These are minor differences.

Both system functions serve the same purpose; they determine the system resolution ability. The broadband system function,  $h_1(x)$ , has a width dependent on the beam size of the laser output, but the monochromatic system function,  $h(x)$ , has a width dependent on the beam size at some distance  $z$  from the laser. Because the beam size widens as the field propagates further from the laser,  $h(x)$  is wider in space than  $h_1(x)$ . Thus the broadband heterodyne system will have better resolution characteristics than either the monochromatic or quasimonochromatic heterodyne systems. All three systems have the same SNR's. Comparing  $h_1(x)$  to  $h_0(x)$ , the broadband direct detection system function, shows that  $h_0(x) = h_1^2(x)$ . It can be shown by Fourier analysis that  $h_0(x)$  is narrower in space than  $h_1(x)$ . Thus the broadband-direct detection system has the best resolution ability of all the systems.

In this chapter, four system models were found. The quasimonochromatic-direct detection and quasimonochromatic-heterodyne current models were shown to be identical to their respective monochromatic models. The broadband systems were found to have better resolution ability than the narrowband systems. The major discovery, however, is that the broadband-

direct detection system does not suffer from speckle effects  
and it has the best resolution ability of all six systems  
investigated.

## V. The Application of the Laser Line-Scan Imaging System to the Ranging Problem

In this thesis, ranging is considered to be the process of determining the height of some point on the rough surface relative to other points on the surface. This process measures macroscopic variations in the surface (on the order of centimeters) as opposed to the microscopic variations in the surface (on the order of the optical wavelength). The laser line-scan imaging system is used to perform the process of ranging.

In this chapter, the method and system used in ranging is discussed first. The selection of the intermediate and carrier frequencies in design considerations is presented. Then the second moment model due to speckle effects is found and quantum noise effects are added to the model. This model is then used to evaluate the system performance for ranging.

### The Ranging Method and System

One method of ranging is to modulate the laser field with a modulation field denoted by

$$m(t) = (1 + \cos 2\pi f_c t)^{\frac{1}{2}} \quad (134)$$

where  $f_c$  is the modulation frequency. During the propagation from the laser to the rough surface and back, the modulation field suffers a time delay of  $2\frac{r_{01}}{c}$ .  $r_{01}$  is shown in Fig. 2 and given by Eq. (12). The laser can be designed with a bandwidth that is narrow enough so that  $r_{01} \cong z$ . This means that any changes in the laser field away from  $z$  are small enough to be ignored. The bandwidth requirement is



$$\frac{1}{B_R} \gg \frac{|\alpha-x|_{\max}^2}{2zc} \quad (135)$$

The time delay is now  $2 \frac{z}{c}$ . The modulation field that is incident on the detector surface is

$$m_d(t) = [1 + \cos 2\pi f_c (t - \frac{2z}{c})]^{1/2} \quad (136)$$

This result is equivalent to the quasimonochromatic case of the previous chapter in that the modulation term is independent of spatial variations.

If the time delay term of Eq. (136) can be isolated, then the distance from individual points on the rough surface to the scanning system can be determined. The system used in determining this distance is a quasimonochromatic laser-heterodyne receiver system. The quasimonochromatic laser is chosen because like an actual laser it has a bandwidth, but it can be modeled by the monochromatic results. The ranging model for this system is developed in the following section.

### The Ranging Model

As with the other models, the field incident on the detector is found first. The mean and covariance of the current are then found. Quantum noise effects are added to the current. The resulting current is processed, as shown in Fig. 8, to determine its amplitude squared. A process is then developed to isolate the time delay term and thus allow the system to be evaluated.

The Modulated Quasimonochromatic Field Incident on the Detector. The modulation term is dependent on time and the propagation distance  $z$ . Thus, this term is not effected by the Huygens-Fresnel integral equation which integrates over spatial coordinates. It can be thought of as a constant during the propagation process. Therefore, the field incident on the detector is the same as for the monochromatic case (Ref Eq. (31)) but now it is multiplied by the time delayed modulation term of Eq. (136). The incident modulated field, denoted  $U_{d,m}(x,t)$  is

$$\begin{aligned}
 U_{d,m}(x,t) &= m_d(t) U_d(x) \\
 &= [1 + \cos 2\pi f_c (t - \frac{2z}{c})]^{1/2} \frac{A}{\lambda z} \exp[-j2(kz - \frac{\pi}{4})] \\
 &\quad \exp[-jk\frac{x^2}{2z}] \int a(\alpha+vt) \exp[j\theta(\alpha+vt)] \exp[-\frac{\alpha^2}{W^2(z)}] \\
 &\quad \exp[-j\frac{k\alpha^2}{z}] \exp[j2\pi\frac{x\alpha}{\lambda z}] d\alpha \tag{137}
 \end{aligned}$$

By algebraic manipulation it can be shown that

$$[1 + \cos 2\pi f_c (t - \frac{2z}{c})]^{1/2} = (2)^{1/2} \cos[2\pi\frac{f_c}{2} (t - \frac{2z}{c})] \tag{138}$$

Therefore, the complex envelope of the field in Eq. (137) is centered about the frequency  $f_c/2$  (recall that the optical frequency,  $f_o$ , is suppressed) and has bandwidth  $B_R$  which is restricted by Eq. (135). A representation of the temporal frequency spectrum of Eq. (137) is shown in Fig. 12a.

The mechanics of the heterodyne system add a local oscillator field to the incident field. The complex envelope of the local

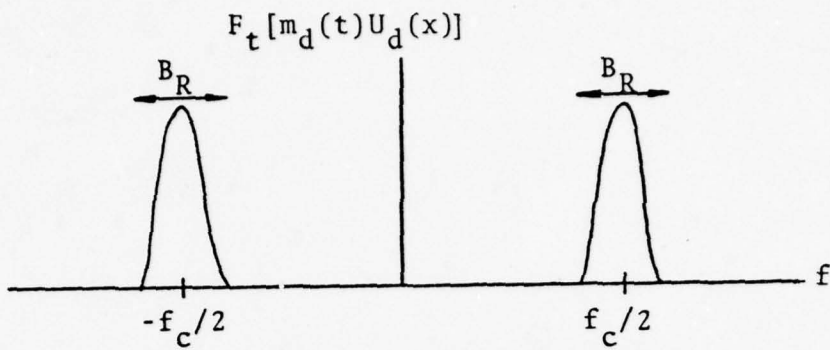


Fig. 12a Temporal Frequency Spectrum of the Detector Field

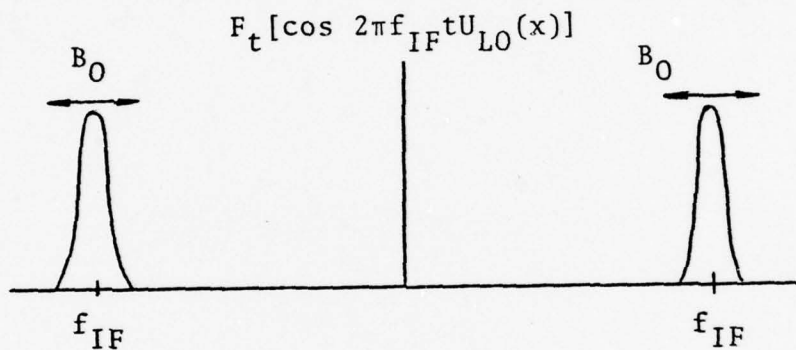


Fig. 12b Temporal Frequency Spectrum of the Local Oscillator Field

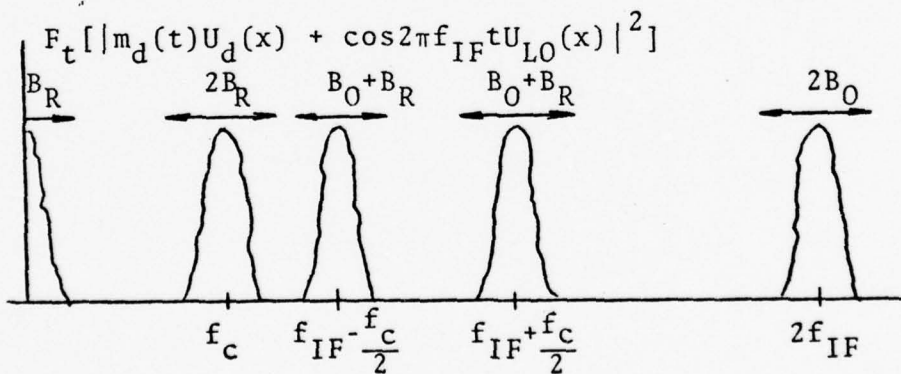


Fig. 12c Temporal Frequency Spectrum of  $|U_{d,m}(x,t) + U_{LO}(x,t)|^2$

Fig. 12 Temporal Frequency Spectrums for the Heterodyne Receiver Fields

oscillator field, denoted  $U_{LO}(\alpha)$ , is centered at the intermediate frequency,  $f_{IF}$ , and it can be thought of as having some narrow bandwidth,  $B_0$ . As shown in Chapter II, the heterodyne current is proportional to the magnitude squared of the sum of the two fields which is

$$\begin{aligned}
 |m_d(t)U_d(x) + \cos[2\pi f_{IF}t]U_{LO}(x)|^2 &= m_d^2(t)|U_d(x)|^2 \\
 &+ (\cos 2\pi f_{IF}t)^2 |U_{LO}(x)|^2 \\
 &+ m_d(t) \cos(2\pi f_{IF}t) 2\text{Re}\{U_d(x)U_{LO}^*(x)\} \\
 = 2[1 + \cos\{2\pi f_c(t - \frac{2z}{c})\}] |U_d(x)|^2 \\
 &+ [1 + \cos(2\pi 2f_{IF}t)] |U_{LO}(x)|^2 \\
 &+ (2)^{\frac{1}{2}} [\cos\{2\pi(f_{IF} + \frac{f_c}{2})(t - \frac{2z}{c})\} + \cos\{2\pi(f_{IF} - \frac{f_c}{2})(t - \frac{2z}{c})\}] \\
 &\quad \text{Re}\{U_d(x)U_{LO}^*(x)\} \tag{139}
 \end{aligned}$$

Fig. 12c is a representation of the one sided temporal frequency spectrum of Eq. (139). Recall that the heterodyne system has a bandpass filter centered near the frequency  $f_{IF}$ . Thus the heterodyne current is dependent on only the last term in Eq. (139). However, the last term contains two signals; one is centered about the frequency  $f_{IF} - \frac{f_c}{2}$  and the other is centered about  $f_{IF} + \frac{f_c}{2}$ . Only one signal is needed. Thus it is arbitrarily

chosen that the signal centered about  $f_{IF} - \frac{f_c}{2}$  is filtered out. This can be done with the use of a bandpass filter with a bandwidth of  $B_R + B_O$  centered at  $f_{IF} + \frac{f_c}{2}$ . The remaining signal is used to determine the heterodyne current.

The signals illustrated in Fig. 12c may overlap with each other depending on the values of  $f_c$ ,  $f_{IF}$ ,  $B_R$ , and  $B_O$ . This overlapping is called aliasing. To prevent aliasing between the signal centered at  $f_{IF} + \frac{f_c}{2}$  and the other signals, the following three conditions must be met:

$$f_{IF} + \frac{f_c}{2} + \frac{1}{2} (B_R + B_O) < 2f_{IF} - B_O \quad (140)$$

$$f_{IF} + \frac{f_c}{2} - \frac{1}{2} (B_R + B_O) > f_c + B_R \quad (141)$$

and

$$f_{IF} + \frac{f_c}{2} - \frac{1}{2} (B_R + B_O) > f_{IF} - \frac{f_c}{2} + \frac{1}{2} (B_R + B_O) \quad (142)$$

These three conditions reduce to two restrictions:

$$f_c > B_R + B_O \quad (143)$$

and

$$f_{IF} > \frac{f_c}{2} + \frac{3}{2} B_R + \frac{1}{2} B_O \quad (144)$$

Fig. 13 is a graph of the possible values of  $f_c$  and  $f_{IF}$  which avoid aliasing between the signal about  $f_{IF} + \frac{f_c}{2}$  and the other signals. The frequency locations in Fig. 12c and the restrictions of Fig. 13 have assumed that  $f_{IF} < f_c$ . Very similar results would have been obtained if it were assumed that  $f_c > f_{IF}$ .

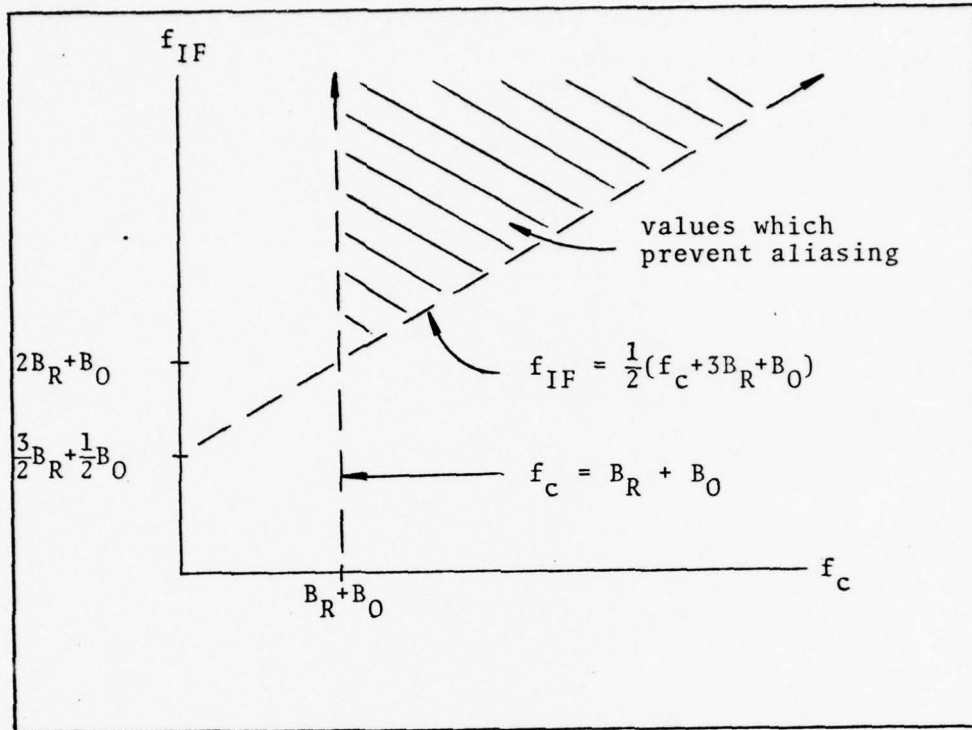


Fig. 13. Values of  $f_{IF}$  and  $f_c$  which Prevent Aliasing

For the restrictions of Eqs. (143) and (144) and for the bandpass filter centered at  $f_{IF} + \frac{f_c}{2}$ , the resulting field is

$$U_{BP}(x,t) = (2)^{\frac{1}{2}} \cos[2\pi(f_{IF} + \frac{f_c}{2})(t - \frac{2z}{c})] \text{Re}\{U_d(x)U_{LO}^*(x)\} \quad (145)$$

This field is centered about  $f_{IF} + \frac{f_c}{2}$  and has bandwidth  $B_R + B_0$ . In this case the value of intermediate frequency is unimportant. Thus by appropriate modulation and filtering techniques, the center frequency of the field can be changed to  $\frac{f_c}{2}$ .

The resulting field still has bandwidth  $B_R + B_0$ , and is

$$\begin{aligned} U_{BP}(x,t) &= (2)^{\frac{1}{2}} \cos\left[2\pi\frac{f_c}{2}\left(t - \frac{2z}{c}\right)\right] \operatorname{Re}\{U_d(x)U_{LO}^*(x)\} \\ &= \operatorname{Re}\{U_{d,m}(x,t)U_{LO}^*(x)\} \end{aligned} \quad (146)$$

where  $U_{d,m}(t)$  was given in Eq. (137). This field is now used to determine the heterodyne receiver current.

The Ranging Current Model. The heterodyne current is found by substituting the bandpassed field of Eq. (146) into Eq. (4). The result is

$$\begin{aligned} i_{h,m}(t) &= \frac{2qn}{hf_0} \frac{A}{\lambda z} [1 + \cos 2\pi f_c(t - \frac{2z}{c})]^{\frac{1}{2}} \operatorname{Re}\{ \\ &\quad \exp[-j2(kz - \frac{\pi}{4})] \int \int \exp[-jk\frac{x^2}{2z}] a(\alpha+vt) \exp[-\frac{\alpha^2}{W^2(z)}] \\ &\quad P_D(x) \exp[-jk\frac{\alpha^2}{z}] \exp[+j2\pi\frac{x\alpha}{\lambda z}] U_{LO}^*(x) dx d\alpha \end{aligned} \quad (147)$$

As with previous heterodyne models, the  $\exp[-jk\frac{x^2}{2z}]$  term can be cancelled by an identical phase term in the local oscillator field. Then the  $x$  integral is just the Fourier transform of the aperture function denoted

$$F_x[P_D(x)] \Big|_{f_x = \frac{\alpha}{\lambda z}} = P_{DF}(\alpha) \quad (148)$$

Also, only the amplitude of the current is of importance here, so the  $\exp[-j2(kz - \frac{\pi}{4})]$  phase term can be neglected. The current

is then written as

$$i_{h,m}(t) = A_3 [1 + \cos 2\pi f_c (t - \frac{2z}{c})]^{1/2} \int P_{DF}(\alpha) a(\alpha + vt) h(\alpha) \exp[j\theta(\alpha + vt)] \exp[-jk \frac{\alpha^2}{z}] d\alpha \quad (149)$$

Comparing Eq. (149) to Eq. (85), it is seen that the modulation heterodyne current, except for the time delayed modulation term, is identical to the monochromatic case and thus the quasimonochromatic case. This term is not random and its amplitude varies between zero and  $(2)^{1/2}$ , thus it does not effect the mean and covariance of the current. They are the same as before:

$$E[i_{h,m}(t)] = 0 \quad (150)$$

and

$$\begin{aligned} C_{i_{h,m}}(t) &= m_d(t)m_d(t') C_{i_h}(t, t') \\ &= A_3^2 [1 + \cos\{2\pi f_c(t - \frac{2z}{c})\}]^{1/2} [1 + \cos\{2\pi f_c(t' - \frac{2z}{c})\}]^{1/2} \\ &\quad \int \int P_{DF}(\alpha) P_{DF}(\alpha') a(\alpha + vt) a(\alpha' + vt') P_\rho(\Delta\alpha + v\Delta t) \\ &\quad h(\alpha) h(\alpha') d\alpha d\alpha' \end{aligned} \quad (151)$$

To make the ranging problem more general, quantum noise effects are now included. Quantum noise is denoted  $n_{TH}(t)$ . It is included by simply adding it to the modulated current of



Eq. (149). This sum, denoted  $i_T(t)$  for total current, is

$$i_T(t) = m_d(t)i_h(t) + n_{TH}(t) \quad (152)$$

The first two moments of the quantum noise due to heterodyne quantum effects are (Ref 26:176)

$$E[n_{TH}(t)] = 0 \quad (153)$$

$$C_{n_{TH}}(t, t') = \frac{q^2 \eta A_d}{hf_o} \delta(t-t') \quad (154)$$

Therefore, the mean and covariance of the total current are

$$\begin{aligned} E[i_T(t)] &= E[i_{h,m}(t)] + E[n_{TH}(t)] \\ &= 0 \end{aligned} \quad (155)$$

and

$$C_{i_h}(t, t') = m_d(t)m_d(t')C_{i_h}(t, t') + C_{n_{TH}}(t, t') \quad (156)$$

It can be seen from Eq. (154), that quantum noise is white noise. That is, its power spectral density has a constant amplitude and exists for all frequencies. One way to decrease the power in the noise is to pass the noise through a bandpass filter. The total current can be passed through a bandpass filter with bandwidth  $B_R + B_O$  centered about  $\frac{f_c}{2}$ . This does not effect the modulated heterodyne current but it does decrease the quantum noise. The bandpassed quantum noise is denoted  $n_{TH, BP}(t)$ .

If  $f_c \gg B_R + B_O$  (possible by system design), the quantum noise can be represented in terms of its quadrature components (Ref 24:237). The quantum noise becomes

$$\begin{aligned} n_{TH,BP}(t) &= n_c(t) \cos(2\pi \frac{f_c}{2} t) - n_s(t) \sin(2\pi \frac{f_c}{2} t) \\ &= r(t) \cos(2\pi \frac{f_c}{2} t + \phi_{TH}(t)) \end{aligned} \quad (157)$$

where

$$r(t) = [n_c^2(t) + n_s^2(t)]^{1/2} \quad (158)$$

and

$$\phi_{TH}(t) = \tan^{-1} \left[ \frac{n_s(t)}{n_c(t)} \right] \quad (159)$$

The quantum noise still has zero mean.

By definition the covariance of the bandpassed quantum noise, now denoted  $C_{TH}(t, t')$ , is

$$\begin{aligned} C_{TH}(t, t') &\triangleq E [n_{TH,BP}(t) n_{TH,BP}(t')] \\ &= E [\cos\{2\pi \frac{f_c}{2} t + \phi_{TH}(t)\} \cos\{2\pi \frac{f_c}{2} t' + \phi_{TH}(t')\} \\ &\quad r(t)r(t')] \end{aligned} \quad (160)$$

The covariance of the total current including bandpassed quantum noise is

$$C_{i_T}(t, t') = m_d(t)m_d(t')C_{i_h}(t, t') + C_{TH}(t, t') \quad (161)$$

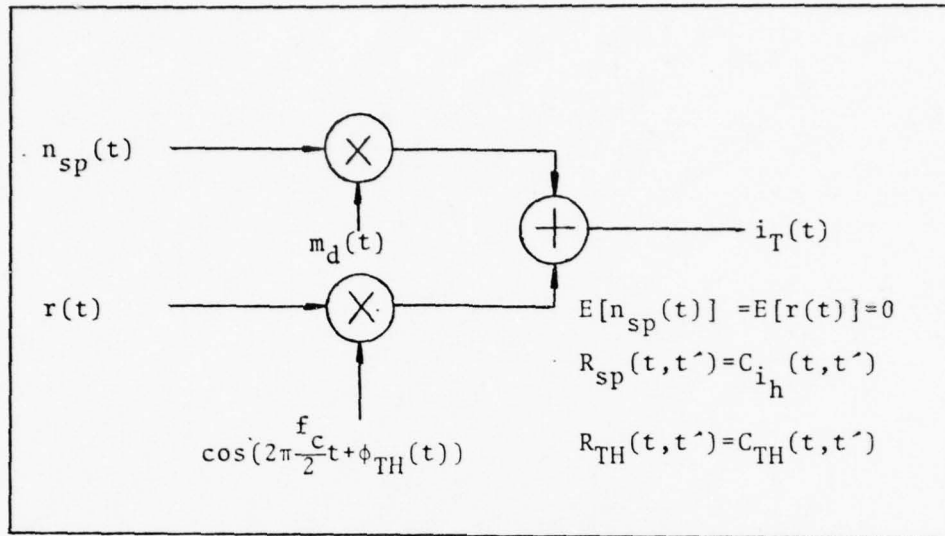


Fig. 14 Model of the Total Current

The noise terms represented by the total current covariance are shown in Fig. 14.

In Eq. (163), the covariance term,  $C_{i_h}(t, t')$ , is not stationary (Ref Eq. (98)). For simplification it is assumed that the surface reflection coefficient,  $a(x)$ , is a constant. This implies that  $C_{i_h}(t, t')$  is stationary and thus Fourier techniques can be used to examine this term. Note that since the quantum noise is stationary, then  $C_{TH}(t, t')$  is stationary also. Eqs. (162) and (163) are used to determine the second moment model for ranging.

The amplitude squared of the total current is found by the process shown in Fig. 8. The first two moments of the amplitude squared are given by Eqs. (90) and (91). They are

$$E[A_T^2(t)] = C_{i_T}(t, t' = t)$$

$$= [1 + \cos\{2\pi f_c(t - \frac{2z}{c})\}] C_{i_h}(t, t' = t) + C_{TH}(t, t' = t) \quad (162)$$

and

$$\begin{aligned} C_{A_T}^2(t, t') &= [C_{i_T}(t, t')]^2 \\ &= [1 + \cos\{2\pi f_c(t - \frac{2z}{c})\}] [1 + \cos\{2\pi f_c(t' - \frac{2z}{c})\}] [C_{i_h}(t, t')]^2 \\ &+ 2[1 + \cos\{2\pi f_c(t - \frac{2z}{c})\}]^{\frac{1}{2}} [1 + \cos\{2\pi f_c(t' - \frac{2z}{c})\}]^{\frac{1}{2}} C_{i_h}(t, t') \\ &\quad C_{TH}(t, t') \\ &+ [C_{TH}(t, t')]^2 \end{aligned} \quad (163)$$

Eq. (162) is the "signal" component of the model. The first term in this equation is composed of two signals: one is centered about zero frequency and the other about  $f_c$ . The amplitude of these two signals is  $C_{i_h}(t, t' = t)$  or  $\sigma_{i_h}^2(t)$ . The last term in Eq. (162) is the variance of the bandpassed quantum noise. This term is centered about zero frequency also (Ref 24:239). If the "signal" terms are A.C. coupled, the terms at zero-frequency are filtered out. This leaves

$$E[A_{T,AC}^2(t)] = \cos[2\pi f_c(t - \frac{2z}{c})] \sigma_{i_h}^2(t) \quad (164)$$

Eq. (163) describes the "noise" components of the model. Let the first term in this equation be denoted  $n_{11}(t)$ . It describes a noise process, call it  $n_{sp}(t)$ , which is zero mean,

has a covariance of  $[C_{i_h}(t, t')]^2$ , and is multiplied by  $[1 + \cos\{2\pi f_c(t - \frac{2z}{c})\}]$ . Multiplication of  $n_{sp}(t)$  by 1 yields a zero frequency term which can also be filtered by A.C. coupling. Fig. 15a is a representation of  $n_{11}(t)$ .

The second term in Eq. (163) describes two statistically independent noise processes,  $n_{12}(t)$  and  $n_{13}(t)$ , which are multiplied together.  $n_{12}(t)$  has zero mean, a covariance of  $C_{i_h}(t, t')$ , and is multiplied by  $[1 + \cos\{2\pi f_c(t - \frac{2z}{c})\}]^{\frac{1}{2}}$ .  $n_{13}(t)$  has zero mean, a covariance of  $C_{i_h}(t, t')$ , and can be represented by the multiplication of  $r(t)$  by  $\cos(2\pi \frac{f_c}{2} t + \phi_{TH}(t))$  (Ref Eq. (16)). Thus the multiplication of  $n_{12}(t)$  and  $n_{13}(t)$ , denoted  $n_{14}(t)$ ,

$$\begin{aligned}
 n_{14}(t) &= n_{12}(t)n_{13}(t) \\
 &= [1 + \cos\{2\pi f_c(t - \frac{2z}{c})\}]^{\frac{1}{2}} \cos(2\pi \frac{f_c}{2} t + \phi_{TH}(t)) n_{12}(t) r(t) \\
 &= \cos[2\pi f_c(t - \frac{z}{c}) + \phi_{TH}(t)] n_{15}(t) \\
 &\quad + \cos[2\pi f_c \frac{z}{c} + \phi_{TH}(t)] n_{15}(t) \tag{165}
 \end{aligned}$$

where  $n_{15}(t) = (\frac{1}{2})^{\frac{1}{2}} n_{12}(t) r(t)$ . The last term in Eq. (165) is at zero frequency since  $\cos(2\pi f_c \frac{z}{c} + \phi_{TH}(t))$  is just some phase shift. Thus as before, this term can be filtered out. The remaining term is represented in Fig. 15b.

The last term in Eq. (163), can be represented by two statistically independent noise processes,  $n_{16}(t)$  and  $n_{17}(t)$ . Each of these is zero mean, has a covariance of  $C_{TH}(t, t')$ , and can be represented by the product of  $r(t)$  and  $\cos(2\pi \frac{f_c}{2} t + \phi_{TH}(t))$

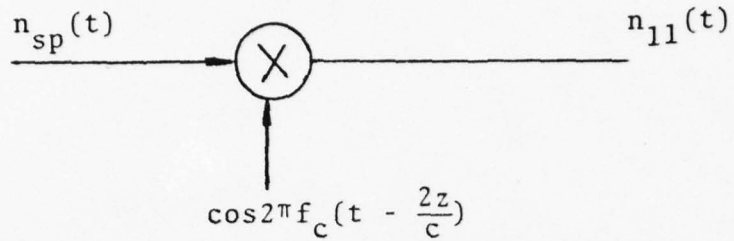


Fig. 15a Speckle Noise Representation

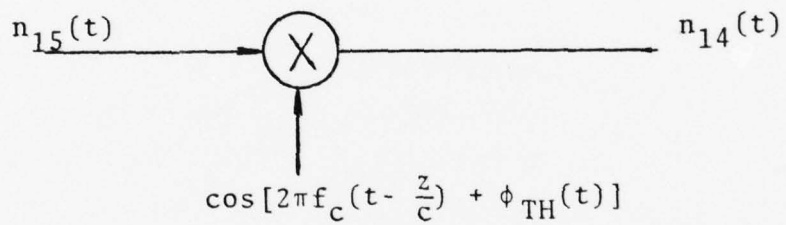


Fig. 15b Speckle-Quantum Noise Representation

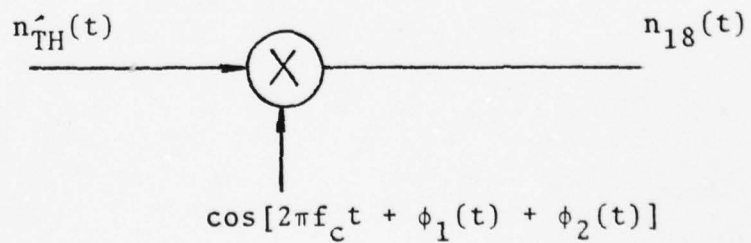


Fig. 15c Quantum Noise Representation

Fig. 15 Noise Representation

The product of  $n_{16}(t)$  and  $n_{17}(t)$  is

$$\begin{aligned}
 n_{18}(t) &= n_{16}(t)n_{17}(t) \\
 &= r_1(t)r_2(t)\cos\left(2\pi\frac{f_c}{2}t + \phi_1(t)\right)\cos\left(2\pi\frac{f_c}{2}t + \phi_2(t)\right) \\
 &= [\cos\{2\pi f_c t + \phi_1(t) + \phi_2(t)\} \\
 &\quad + \cos\{\phi_1(t) - \phi_2(t)\}] n_{TH}(t) \tag{166}
 \end{aligned}$$

where  $n_{TH}(t) = \frac{1}{2}r_1(t)r_2(t)$ . Once again the last term in Eq. (166) is centered about zero frequency since  $\cos(\phi_1(t) - \phi_2(t))$  is only a phase shift. Thus this term is filtered out. The remaining term is shown in Fig. 15c.

A representation of the "signal" and "noise" terms described by Eqs. (162) and (163) has now been suggested. Thus from a second moment model standpoint, it can be said that the amplituded squared of the total A.C. coupled current is

$$\begin{aligned}
 A_{T,AC}^2(t) &= \cos^2 2\pi f_c \left(t - \frac{Z}{c}\right) \sigma_{ih}^2(t) \\
 &\quad + \cos^2 2\pi f_c \left(t - \frac{Z}{c}\right) n_{sp}(t) \\
 &\quad + \cos[2\pi f_c \left(t - \frac{Z}{c}\right) + \phi_{TH}(t)] n_{15}(t) \\
 &\quad + \cos[2\pi f_c t + \phi_1(t) + \phi_2(t)] n_{TH}(t) \tag{167}
 \end{aligned}$$

Eq. (167) is now referred to as the ranging current. Fig. 16 is a diagram of the second moment model of the ranging current.

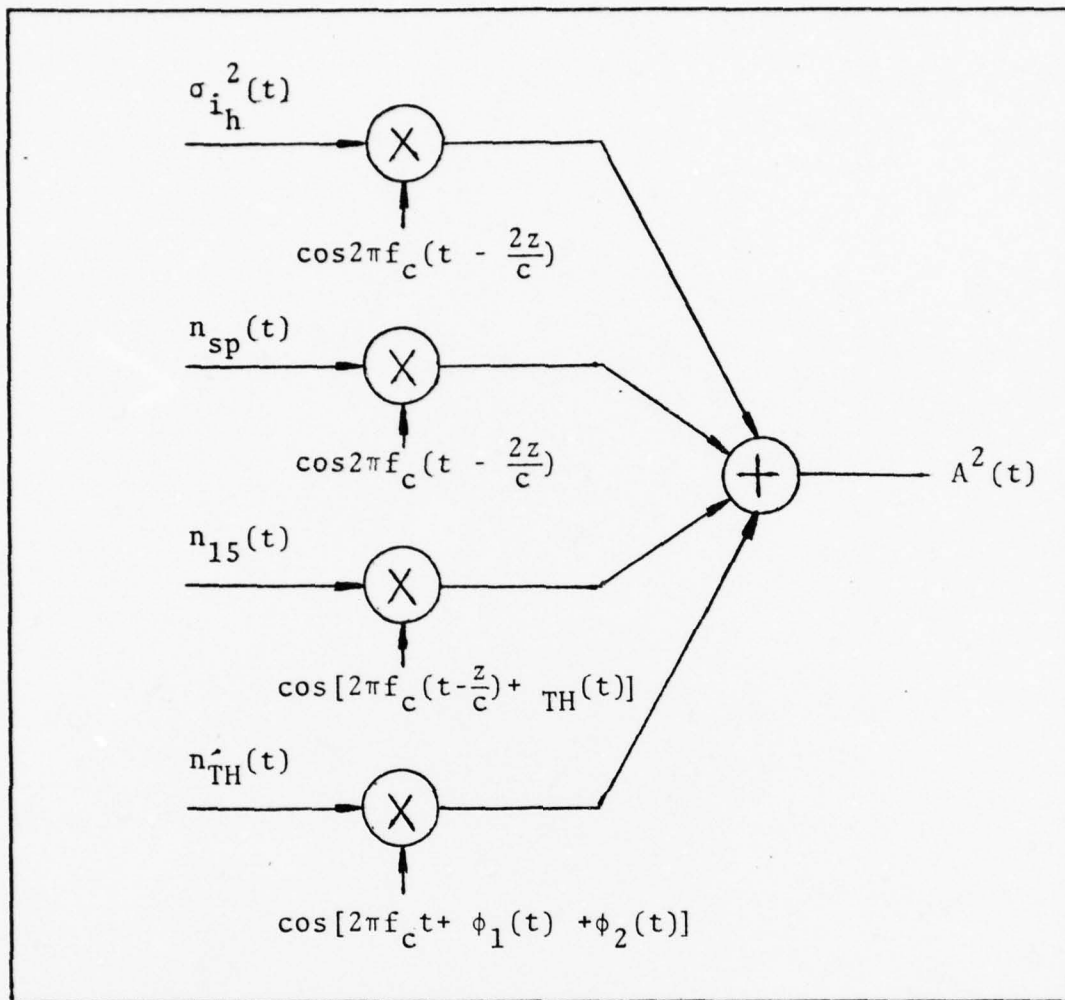


Fig. 16 The Current Model for Ranging

With the help of Eq. (167) and the current model, it is possible to detect the time delay,  $\frac{2z}{c}$ . This is done in the following section.

Detection of the Time Delay. It is desired to measure the time delay so that the distance from the rough surface to the imaging system can be obtained. What is actually measured though is the phase delay that results in the field as it propagates down and back up. Measuring the phase delay, which



is  $2\pi f_c \frac{2z}{c}$ , is good enough since  $f_c$  and  $c$  are known. Thus,  $z$ , the distance that is desired to be known, is the only unknown and can be easily determined from the phase delay. However, because quantum and speckle noise are present, the phase delay that is measured includes the phase delay of the noises as well as the laser field's phase delay. Therefore there is an error in the value of  $z$  that is measured. The phase delay error can be seen from a phase diagram of the ranging current in Eq. (167). First, this current must be rearranged.

Consider the third term in Eq. (167). It can be rewritten as

$$\begin{aligned}
 \cos[2\pi f_c (t - \frac{z}{c}) + \phi_{TH}(t)] n_{15}(t) &= \cos[2\pi f_c (t - \frac{2z}{c}) + (2\pi f_c \frac{z}{c} \\
 &\quad + \phi_{TH}(t))] n_{15}(t) \\
 &= \cos 2\pi f_c (t - \frac{2z}{c}) \cos[2\pi f_c \frac{z}{c} + \phi_{TH}(t)] n_{15}(t) \\
 &\quad + \sin[2\pi f_c (t - \frac{2z}{c})] \sin[2\pi f_c \frac{z}{c} + \phi_{TH}(t)] n_{15}(t) \quad (168)
 \end{aligned}$$

The last term in Eq. (167), can be rewritten

$$\begin{aligned}
 \cos[2\pi f_c t + \phi_1(t) + \phi_2(t)] n'_{TH}(t) \\
 &= \cos[2\pi f_c (t - \frac{2z}{c}) + 2\pi f_c \frac{2z}{c} + \phi_3(t)] n'_{TH}(t) \\
 &= \cos[2\pi f_c (t - \frac{2z}{c})] \cos[2\pi f_c \frac{2z}{c} + \phi_3(t)] n'_{TH}(t) \\
 &\quad + \sin[2\pi f_c (t - \frac{2z}{c})] \sin[2\pi f_c \frac{2z}{c} + \phi_3(t)] n'_{TH}(t) \quad (169)
 \end{aligned}$$

where  $\phi_3(t) = \phi_2(t) + \phi_1(t)$ . Now the ranging current becomes

$$\begin{aligned}
 A^2(t) = & [\sigma_{i_h}^2(t) + n_{sp}(t) + \cos\{2\pi f \frac{z}{c} + \phi_{TH}(t)\} n_{15}(t) \\
 & + \cos\{2\pi f \frac{2z}{c} + \phi_3(t)\} n'_{TH}(t)] \cos 2\pi f_c (t - \frac{2z}{c}) \\
 & + [\sin\{2\pi f \frac{z}{c} + \phi_{TH}(t)\} n_{15}(t) + \sin\{2\pi f \frac{2z}{c} + \phi_3(t)\} n'_{TH}(t)] \\
 & \sin 2\pi f_c (t - \frac{2z}{c}) \quad (170)
 \end{aligned}$$

A phase diagram of Eq. (170) is plotted in Fig. 17.

In Fig. 17 the desired phase to be measured is  $2\pi f_c \frac{2z}{c}$ . Due to noise, the phase that is actually measured is  $2\pi f_c \frac{2z}{c} + \phi_e$ , where  $\phi_e$  is the phase error or deviation due to noise.

The phase deviation is written as

$$\phi_e = \tan^{-1} \left[ \frac{n'_{TH}(t) \sin \theta_1 + n_5(t) \sin \theta_2}{\sigma_{i_{TH}}^2 + n_{sp}(t) + n'_{TH}(t) \cos \theta_1 + n_{15}(t) \cos \theta_2} \right] \quad (171)$$

where

$$\theta_1 = 2\pi \frac{f_c}{2} \frac{2z}{c} + \phi_3(t) \quad (172)$$

and

$$\theta_2 = 2\pi \frac{f_c}{2} \frac{z}{c} + \phi_{TH}(t) \quad (173)$$

Eq. (171) is not very enlightening. It becomes somewhat clearer if looked at in its two limiting cases: (1) speckle noise dominant and (2) quantum noise dominant. Each of these cases is discussed below.

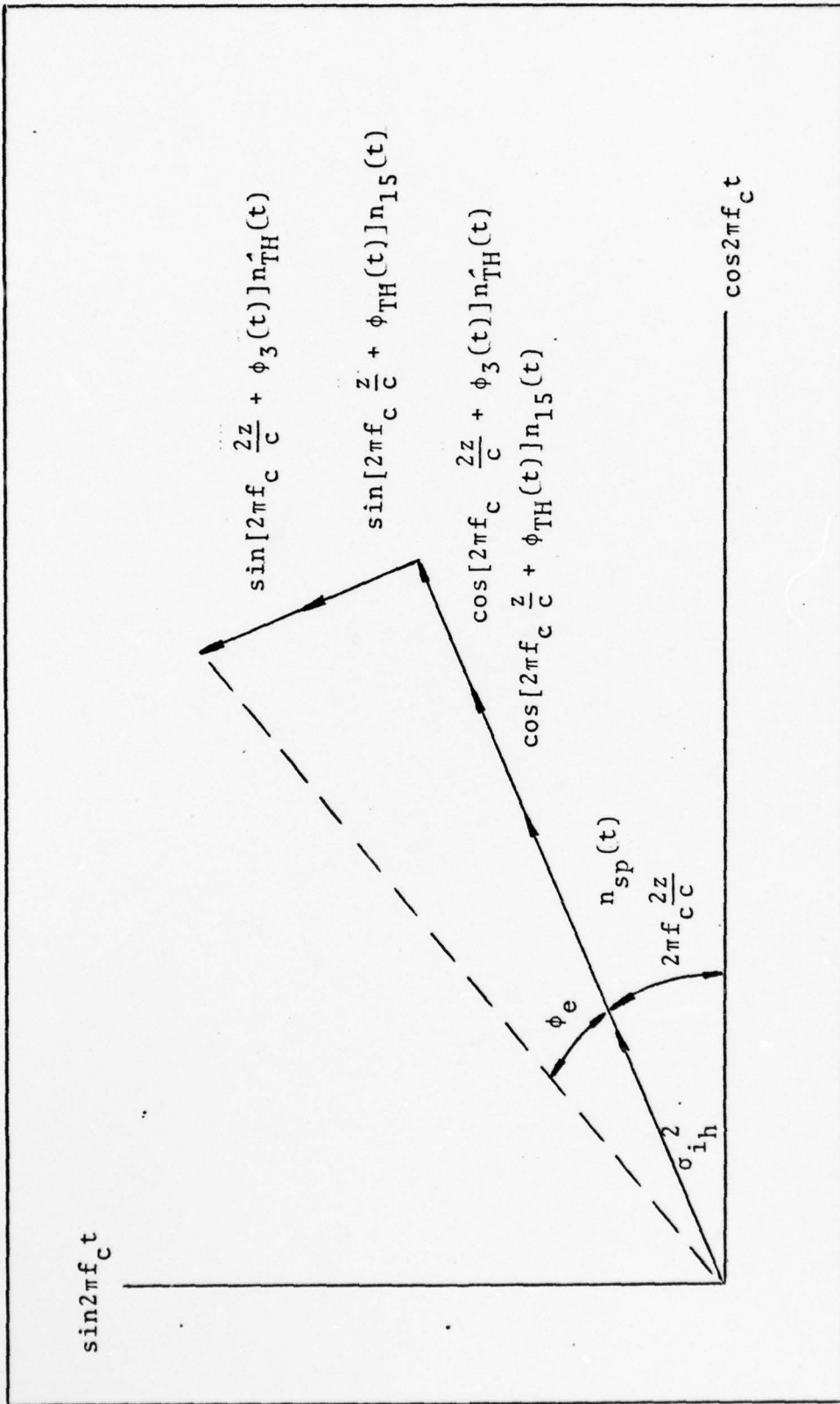


Fig. 17 Phase Diagram of the Ranging Current

If speckle noise is dominant over quantum noise, then all quantum noise terms can be neglected and the phase deviation is due to speckle noise.

In Eq. (171), the  $n_{TH}'(t)$  and  $n_{15}(t)$  terms are due, at least in part, to quantum noise. If they are neglected, the phase deviation due to speckle noise is

$$\phi_{sp} = \tan^{-1} \left[ \frac{0}{n_{sp}(t) + \sigma_{i_h}^2(t)} \right] = 0 \quad (174)$$

From the last equation it appears that the phase of the laser field can be measured exactly for speckle noise limited systems. This seems intuitive because the speckle noise, like the laser field, is propagated from the surface to the imaging system. Since both take the same path, they should suffer the same delay. Most imaging systems are speckle noise limited therefore, it appears they should work well for ranging.

On the other hand, if quantum noise is dominant, the  $n_{sp}(t)$  and  $n_{15}(t)$  terms are neglected ( $n_{15}(t)$  results from the cross correlation of the speckle and quantum noise, thus it is neglected for both cases). The phase deviation due to quantum noise is

$$\phi_{TH} = \tan^{-1} \left[ \frac{n_{TH}'(t)\sin\theta_1}{\sigma_{i_{TH}}(t) + n_{TH}'\cos\theta_1} \right] \quad (175)$$

This result is very similar to the result obtained by Ziemer and Tranter (Ref 24:277-278) for the case of angle demodulation in the presence of noise. (Eq. 175) does not indicate the magnitude of the phase error, but it does imply that some deviation occurs. It can be seen that for  $\sigma_{i_{TH}}(t) \gg n_{TH}'$ , the phase deviation is small. If the mean and covariance of Eq. (175) are found, then the deviation can be better understood. However, that is beyond the scope of this thesis.

One practical consideration which should be taken into consideration for both cases is that phase detectors are amplitude dependent. All the components which make up the phase deviation term (Ref Eq. (171)) have random amplitudes. Therefore, the results of both cases are true only for a carefully designed phase detector which is insensitive to amplitude variations of the signal.

The important result of this chapter is that it appears that laser line-scan imaging systems can be effectively used for ranging. The only assumptions used in showing this were:

- (1) the bandwidth of the laser source is narrow enough that laser field, at any point in space, is constant across its width and
- (2) the imaging system is speckle noise limited. Neither one of these are severe restrictions. Also important is Fig. 13. It gives the values of  $f_{IF}$  and  $f_c$  that can be used to avoid aliasing. This insures that the correct image is processed by the system.

## VI. Conclusion

### Summary

The effects of speckle on the output current of an imaging system were examined. The imaging system was composed on a laser scanning a rough surface (compared to the laser wavelength) and a receiver measuring the field reflected from the surface. Three types of lasers and two types of receivers were examined. The lasers were designated by their bandwidths as monochromatic, quasimonochromatic, and broadband. The two receivers were the direct detection and heterodyne.

The field reflected from the rough surface was "crudely" modeled by multiplying the incident laser field by a reflectance term and a random phase term. The reflectance term was the desired quantity or "signal" to be measured. The phase term simulated the effects of speckle. All fields were propagated by the Huygens-Fresnel integral.

The system composed of a monochromatic laser and a direct detection receiver was examined first. A system function dependent on the laser beam spot size at the surface was defined. It was shown that the resolution ability of the system was determined by the width of the system function. By second moment techniques, the "noise" (due to speckle effects) measured by the system was found to be signal dependent. The significance of this result was that the signal to noise ratio (SNR) could not be improved by increasing the signal power. The value of the SNR was shown to be greater than or equal to one. The far field and near field cases were found to be identical. The monochromatic laser was then replaced by a quasimonochromatic one.

The results for this new system were shown to be identical to the monochromatic results.

For the imaging system consisting of a heterodyne receiver and a monochromatic laser, the measured "noise" due to the effects of speckle was also found to be signal dependent. Thus the SNR, which was equal to one, could not be improved by increasing the signal power. The resolution of the system was shown to vary with the beam spot size at the surface and the spatial fourier transform of the receiver's detection area. The far and near field cases were identical. The heterodyne results were unchanged when the monochromatic laser was replaced by a quasimonochromatic one. When a broadband laser was used, the only result which changed was that the resolution ability of the heterodyne system improved.

The most significant results occurred when the imaging system was composed of a direct detection receiver and a broadband laser. It was shown that this system is not effected by speckle noise. This was different from all other systems. They were limited by speckle effects. This system was found to have the best resolution characteristics of all the systems investigated. From these results, it was determined that this system is the optimum system to use for laser line-scan imaging.

As an application, the system consisting of a quasimonochromatic laser and heterodyne receiver was used for ranging. In addition to the effects of speckle, quantum effects were included. The laser field was amplitude modulated. The phase delay in the modulation term of the reflected field was measured and

used to determine the distance from the surface to the system. However, the measured phase delay included a phase error due to quantum and speckle effects. It was shown that for the case of speckle noise dominate over quantum noise, the phase delay could be accurately measured. For the case of quantum noise dominate, it was found that an error would result in the measured phase delay. No attempt was made to quantify this error. It was noted that the obtained results were only valid for a phase detector which is insensitive to amplitude variations. It was concluded that ranging could be effectively performed. A method for selecting the intermediate and carrier frequencies used in the ranging problem was also presented.

#### Recommendations

In this thesis, a laser line-scan imaging system was modeled for different combinations of laser sources and receivers. These models were based on theoretical analysis. It is recommended that these models be compared to experimental data to test their validity.

One calculation used to determine the effects of speckle on broadband imaging systems (Ref Eq. (123)) was only an approximation. It seems feasible that this calculation can be quantified by comparison to the analysis of similar calculations. This would add to the understanding of the broadband results in this paper.

In the ranging problem, the phase error was presented but not analyzed. A statistical analysis of the phase error would result in a better understanding in the magnitude of the error and the variations in its amplitude. As previously stated,



phase detectors are amplitude dependent. A statistical analysis would indicate the effect of amplitude variations on phase detectors. Also, the ranging problem was examined for the case of a constant surface reflection coefficient. If the problem were solved for a spatially varying coefficient, a more general solution would be obtained.

## Bibliography

1. Journal of the Optical Society of America, 66: (November 1976).
2. George, Nicholas. "Speckle," Optics News, 2: 14-20 (January 1976).
3. Holmes, Fred J., et. al. Experimental Pulse Laser Remote Crosswind Measurement System -- Feasibility Study and Design (Part IV). Research and Development Technical Report FA-TR-76065. Department of Applied Physics and Electronic Science, The Oregon Graduate Center, Beaverton, Oregon, November 1976. (ADA 038638).
4. Newton, Issac, Opticks, (Reprinted by Dover Press, New York, 1952), 1730.
5. Dainty, J.C., et. al. Laser Speckle and Related Phenomena. New York: Springer-Verlag, 1975.
6. Rigden, J.D. and E.I. Gordon. "Granularity of Scattered Optical Maser Light." Proceeding I.R.E., 50: 2367-2368 (October-December 1962).
7. Oliver, B.M. "Sparkling Spots and Random Diffraction." Proceedings IEEE, 51: 220-221 (January-March 1963).
8. Jacobs, S. F. and Rabinowitz, P. J. "Optical Heterodyning with a CW Gaseous Laser" in Quantum Electronics Proceeding of the Third International Congress (1963), edited by P. Grivet and N. Bloembergen. New York: Columbia University Press, 1964.
9. Pratt, William K. Laser Communication Systems. New York: John Wiley and Sons, Inc., 1969.
10. Davenport, W. B. Jr. Probability and Random Processes. St. Louis: McGraw Hill Book Company, 1970.
11. Papoulis, A. Probability, Random Variables, and Stochastic Processes. St. Louis: McGraw-Hill Book Company, 1965.
12. Goodman, J. W. Introduction to Fourier Optics. St. Louis: McGraw-Hill Book Company, 1971.
13. Papoulis, A., Systems and Transforms with Applications in Optics. St. Louis: McGraw-Hill Book Company, 1968.
14. Siegman, A. E. An Introduction to Lasers and Masers. St. Louis: McGraw-Hill Book Company, 1971.

AD-A064 048

AIR FORCE INST OF TECH WRIGHT-PATTERSON AFB OHIO SCH--ETC F/G 17/8  
AN ANALYSIS OF THE EFFECTS OF SPECKLE ON LASER SCANNING SYSTEMS--ETC(U)  
DEC 78 B W NEWTON

UNCLASSIFIED

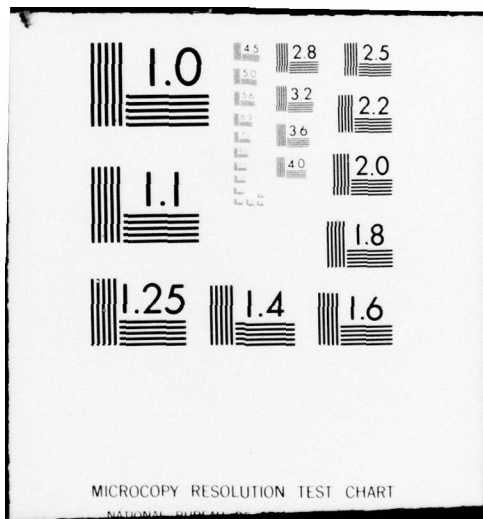
AFIT/GEO/EE/78-3

NL

2 of 2  
AD  
A064048



END  
DATE  
FILMED  
3-79  
DDC



MICROCOPY RESOLUTION TEST CHART

NATIONAL BUREAU OF STANDARDS-1963-A

15. Papoulis, A. The Fourier Integral and its Applications. St. Louis: McGraw-Hill Book Company, 1962.
16. Lyons, B. W. A Speckle Noise Model for Optical Heterodyne Line-Scan Imagery. Masters Thesis, School of Engineering, AirForce Institute of Technology, Wright-Patterson AFB, Ohio, 1977.
17. Beckman, P. and Spizzichino, A., The Scattering of Electromagnet Waves From Rough Surfaces. New York: The MacMillan Company, 1963.
18. Goodman, J. W. "Some Effects of Target-Induced Scintillation on Optical Radar Performance." Proceedings of the IEEE, 53: 1688-1700 (November 1965).
19. Miller, M. G., et. al. "Second Order Statistics of Laser Speckle Patterns." Journal of the Optical Society of America, 65: 779-785 (July 1975).
20. Fujii, H. and T. Asakura. "Effect of Surface Roughness on the Statistical Distribution of Image Speckle Intensity." Optics Communications, 11: 34-38 (May 1974).
21. Pederson, H. M. "Object Roughness Dependence of Partially Developed Speckle Patterns in Coherent Light." Optics Communications, 16: 63-67 (January 1976).
22. Kurtz, C.N. "Transmittance Characteristics of Surface Diffusers and Design of Nearly Band-Limited Binary Diffusers." Journal of the Optical Society of America, 62: 982-989 (August 1972)
23. Reed, I. S. "On a Moment Theorem for Complex Gaussian Processes." IRE Transactions on Information Theory, 8: 194-195 (April 1962).
24. Ziemer, R. E. and W. H. Tranter. Principles of Communications. Boston: Houghton Mifflin Company, 1976.
25. Klauder, J. R., et. al. "The Theory and Design of Chirp Radars." The Bell System Technical Journal, 39: 745-808 (July 1969).
26. Gagliardi, R. M. and S. Karp. Optical Communications. New York: John Wiley and Sons, 1976.
27. Cook, C. E. and M. Bernfeld. Radar Signals. New York: Academic Press, 1967.
28. Fowle, E. N. "The Design of FM Pulse-Compression Signals." IEEE Transactions on Information Theory, 10: 61-67 (1964)

## Appendix A

### Extended Huygens-Fresnel Integral

Recall from the section on complex representation that the real scalar optical field is

$$u(\bar{r}, t) = A(\bar{r}, t) \cos[2\pi f_0 t - \phi(\bar{r}, t)] \quad (\text{A-1})$$

and its complex envelope (with  $\exp[-j2\pi f_0 t]$  time dependence) is

$$U(\bar{r}, t) = A(\bar{r}, t) \exp[j\phi(\bar{r}, t)] \quad (\text{A-2})$$

where  $\bar{r}$  is a vector with spatial coordinates  $(x, y)$ . Let the temporal Fourier transform of Eqs. (A-1) and (A-2) be denoted

$$F_t[u(\bar{r}, t)] = V(\bar{r}, f) \quad (\text{A-3})$$

and

$$F_t[U(\bar{r}, t)] = V_{LP}(\bar{r}, f) \quad (\text{A-4})$$

By Fourier analysis techniques it can be shown that Eq. (A-3) can be written in terms of Eq. (A-4) as

$$\begin{aligned} V(\bar{r}, f) &= \frac{1}{2} F_t[U^*(\bar{r}, t) \exp(j2\pi f_0 t)] \\ &+ \frac{1}{2} F_t[U(\bar{r}, t) \exp(-j2\pi f_0 t)] \end{aligned} \quad (\text{A-5})$$

For the case where the complex envelope,  $U(\bar{r}, t)$ , is monochromatic, the Fourier transform of the optic field can be written

$$V(\bar{r}, f) = V(\bar{r}, f_0) \delta(f - f_0) + V(\bar{r}, -f_0) \delta(f + f_0) \quad (\text{A-6})$$

The amplitude of the last term in Eq. (A-6) is

$$\begin{aligned} V(\bar{r}, -f_0) &= \frac{1}{2} F_t [U(\bar{r}, t) \exp(-j2\pi f_0 t)] \\ &= \frac{1}{2} V_{LP}(\bar{r}, f + f_0) \end{aligned} \quad (\text{A-7})$$

The two dimensional form of the Huygens-Fresnel integral is

$$U_1(\bar{r}_1) = \frac{\exp[jkz]}{j\lambda z} \iint U(\bar{r}) \exp[j\frac{k}{2z} |\bar{r}_1 - \bar{r}|^2] d\bar{r} \quad (\text{A-8})$$

where  $\lambda = c/f_0$ . On comparing Eqs. (A-5) and (A-7) it is seen that Eq. (A-8) can be written as

$$V_1(\bar{r}_1, -f_0) = \frac{\exp[jkz]}{j\lambda z} \iint V(\bar{r}, -f_0) \exp[j\frac{k}{2z} |\bar{r}_1 - \bar{r}|^2] d\bar{r} \quad (\text{A-9})$$

After completing a change of variables  $f = -f_0$ , Eq. (A-9) becomes

$$V_1(\bar{r}_1, f) = \frac{\exp[-j2\pi z \frac{f}{c}]}{-j\frac{c}{f} z} \iint V(\bar{r}, f) \exp[-j\frac{k}{2z} |\bar{r}_1 - \bar{r}|^2] d\bar{r} \quad (\text{A-10})$$

This equation is valid for propagation of any field component at frequency  $f$ . To express the results in terms of complex envelopes, note that for all frequencies  $f$  near  $-f_0$

$$V(\bar{r}, f) = \frac{1}{2} V_{LP}(\bar{r}, f + f_0) \quad (\text{A-11})$$

Substituting Eq. (A-11) into Eq. (A-10) yields

$$V_{1,LP}(\bar{r}_1, f + f_0) = \frac{f \exp[-j2\pi z \frac{f}{c}]}{-jcz} \iint V_{LP}(\bar{r}, f + f_0) \exp[-j \frac{\pi f}{zc} |\bar{r}_1 - \bar{r}|^2] d\bar{r} \quad (A-12)$$

The temporal inverse fourier transform of Eq. (A-12) is

$$U_1(\bar{r}, t) e^{-j2\pi f_0 t} = \frac{1}{2\pi z c} \iint \frac{d}{dt} \left\{ U(\bar{r}, t - \frac{z}{c} - \frac{|\bar{r}_1 - \bar{r}|^2}{2zc}) \exp[-j2\pi f_0 (t - \frac{z}{c} - \frac{|\bar{r}_1 - \bar{r}|^2}{2zc})] \right\} d\bar{r} \quad (A-13)$$

By use of the chain rule, Eq. (A-13) becomes

$$U_1(\bar{r}_1, t) = \frac{1}{2\pi z c} \exp[jkz] \iint \exp[j \frac{k}{2z} |\bar{r}_1 - \bar{r}|^2] \left\{ \frac{d}{dt} U(\bar{r}, t - \frac{z}{c} - \frac{|\bar{r}_1 - \bar{r}|^2}{2zc}) - j2\pi f_0 U(\bar{r}, t - \frac{z}{c} - \frac{|\bar{r}_1 - \bar{r}|^2}{2zc}) \right\} d\bar{r} \quad (A-14)$$

Eq. (A-14) can be simplified somewhat. If it is assumed that the bandwidth of  $U(\bar{r}, t)$  is much less than the optical frequency  $f_0$ , then the  $f$  in the numeration of Eq. (A-12) can be approximated by  $f_0$ . The resulting temporal inverse Fourier transform of Eq. (A-12) is then

$$U_1(\bar{r}, t) = \frac{\exp[jkz]}{j\lambda z} \iint U_1(\bar{r}, t - \frac{z}{c} - \frac{|\bar{r}_1 - \bar{r}|^2}{2zc}) \exp[j \frac{k}{2z} |\bar{r}_1 - \bar{r}|^2] d\bar{r} \quad (A-15)$$



This assumption implies that the field does not change significantly in time relative to the variation at  $f_0$ . Eq. (A-15) would also result is the derivative term in Eq. (A-14) was assumed to be insignificant in comparison to the other term in that equation.

Another simplification can be made to Eq. (A-14) when the bandwidth of  $U(r,t)$  is restricted by

$$\frac{1}{B} \gg \frac{|\dot{r}_{01}|_{\max}}{c} \quad (\text{A-16})$$

where  $r_{01}$  is defined by Eq. (10). This is the quasimonochromatic restriction (Ref 12:108). The resulting Huygens-Fresnel integral, which is valid for quasimonochromatic fields, is

$$U_1(\bar{r}_1, t) = \frac{\exp[jkz]}{j\lambda z} \iint U(\bar{r}, t) \exp[j\frac{k}{2z} |\bar{r}_1 - \bar{r}|^2] d\bar{r} \quad (\text{A-17})$$

The Huygens-Fresnel integral, which is valid for monochromatic fields, has been extended so that it is valid for fields of any bandwidth (Ref Eq. (A-14)). Two special cases, the broadband and quasimonochromatic, were presented. The propagation of broadband fields is given by Eq. (A-15) and the propagation of quasimonochromatic fields is given by Eq. (A-17).

## Appendix B

### The Method of Stationary Phase

The method of stationary phase is an asymptotical approximation to the solution of an integral. It is discussed by Papoulis in two of his books (Ref 13: 234-250, 15:139-143). The method is summarized below.

Consider the integral

$$Q(\Delta f) = \int_R \int g_1(\alpha, \beta) \exp[j\Delta f g_2(\alpha, \beta)] d\alpha d\beta \quad (\text{B-1})$$

where  $R$  is a region in the  $\alpha, \beta$  plane.  $g_2(\alpha, \beta)$  must be twice differentiable in  $R$ . The extreme value of  $g_2(\alpha, \beta)$  at a single point  $(\alpha_0, \beta_0)$  in  $R$  is found by the first partial derivatives of  $g_2(\alpha, \beta)$ :

$$\frac{\partial g_2(\alpha, \beta)}{\partial \alpha} = 0 \triangleq g_{2,\alpha}(\alpha_0, \beta_0) \quad (\text{B-2})$$

$$\frac{\partial g_2(\alpha, \beta)}{\partial \beta} = 0 \triangleq g_{2,\beta}(\alpha_0, \beta_0) \quad (\text{B-3})$$

If  $g_1(\alpha, \beta)$  is continuous at  $(\alpha_0, \beta_0)$  and if

$$g_{2,\alpha\alpha} g_{2,\beta\beta} - (g_{2,\alpha\beta})^2 \neq 0 \quad (\text{B-4})$$

and

$$g_{2,\beta\beta} \neq 0 \quad (\text{B-5})$$

where  $g_{2,\alpha\alpha}$ ,  $g_{2,\beta\beta}$ , and  $g_{2,\alpha\beta}$  are the partial derivatives evaluated at  $(\alpha_0, \beta_0)$ , then as  $\Delta f$  approaches infinity

$$Q(\Delta f) = \frac{j2\pi g_1(\alpha_0, \beta_0)}{\Delta f [g_{2,\alpha\alpha} g_{2,\beta\beta} - g_{2,\alpha\beta}^2]^{\frac{1}{2}}} \exp[j\Delta f g_2(\alpha_0, \beta_0)] \quad (B-6)$$

## Vita

Billy W. Newton, Jr., was born on 7 December 1954 in Sylvania, Georgia. He graduated from Screven County High School in 1973. He attended the Georgia Institute of Technology from 1973 to 1977 from which he received the degree of Bachelor of Electrical Engineering. Upon graduation, he received a commission in the USAF through the ROTC program and entered active duty on 4 July 1977, as a student in the School of Engineering, Air Force Institute of Technology.

Permanent Address: 401 South Main St.  
Sylvania, Georgia 30467

UNCLASSIFIED

SECURITY CLASSIFICATION OF THIS PAGE (When Data Entered)

REPORT DOCUMENTATION PAGE		READ INSTRUCTIONS BEFORE COMPLETING FORM
1. REPORT NUMBER AFIT/GEO/EE/78-3	2. GOVT ACCESSION NO.	3. RECIPIENT'S CATALOG NUMBER
4. TITLE (and Subtitle) AN ANALYSIS OF THE EFFECTS OF SPECKLE ON LASER SCANNING SYSTEMS		5. TYPE OF REPORT & PERIOD COVERED MS THESIS
		6. PERFORMING ORG. REPORT NUMBER
7. AUTHOR(s) Billy W. Newton, Jr. 2nd Lt., USAF		8. CONTRACT OR GRANT NUMBER(s)
9. PERFORMING ORGANIZATION NAME AND ADDRESS Air Force Institute of Technology Wright-Patterson AFB, Ohio 45433		10. PROGRAM ELEMENT, PROJECT, TASK AREA & WORK UNIT NUMBERS
11. CONTROLLING OFFICE NAME AND ADDRESS Electro-Optics and Reconnaissance Branch Air Force Avionics Laboratory Wright-Patterson AFB, Ohio 45433		12. REPORT DATE
		13. NUMBER OF PAGES 103
14. MONITORING AGENCY NAME & ADDRESS (if different from Controlling Office)		15. SECURITY CLASS. (of this report)  UNCLASSIFIED
		15a. DECLASSIFICATION/DOWNGRADING SCHEDULE
16. DISTRIBUTION STATEMENT (of this Report) Approved for public release; distribution unlimited		
17. DISTRIBUTION STATEMENT (of the abstract entered in Block 20, if different from Report)		
18. SUPPLEMENTARY NOTES Approved for public release; IAW AFR 190-17 JOSEPH P. HIPPS, Major, USAF Director of Information 1-23-79		
19. KEY WORDS (Continue on reverse side if necessary and identify by block number) Line scanning                      Speckle Ranging                              Laser scattering Heterodyne detection              Rough surfaces Direct detection                      Broadband lasers		
20. ABSTRACT (Continue on reverse side if necessary and identify by block number) The effects of speckle on an imaging system composed of a laser scanning a rough surface and a receiver measuring the reflected field are examined. Three types of lasers and two types of receivers are considered. The lasers are designated by their bandwidths as monochromatic, quasimonochromatic, and broadband. The receivers are the heterodyne and direct detection.  A second moment model is obtained for each system. The system		

UNCLASSIFIED

SECURITY CLASSIFICATION OF THIS PAGE(When Data Entered)

consisting of a broadband laser and direct detection receiver is shown to be independent of speckle effects. All other systems are shown to have a "noise", due to speckle, which is signal dependent. The signal to noise ratio for the direct detection system is shown to be higher than for the heterodyne systems. The system with broadband lasers are found to have a higher resolution than systems with other laser sources.

In addition, a system consisting of a quasimonochromatic laser and heterodyne receiver is used for ranging. The phase delay in the reflected laser field is measured to determine the range from the system to a surface. It is found that the ranging performance of a heterodyne scanning system is not fundamentally degraded by speckle effects.

UNCLASSIFIED

SECURITY CLASSIFICATION OF THIS PAGE(When Data Entered)